

SUPPORTING INFORMATION

Supporting Information

Enabling Dynamic Ultralong Organic Phosphorescence in Molecular Crystals by Synergy of Intramolecular and Intermolecular Interactions

Zhan Yang, Eethamukkala Ubba, Qiuyi Huang, Zhu Mao,* Wenlang Li, Junru Chen, Juan Zhao,* Yi Zhang and Zhenguo Chi*

Abstract: Ultralong organic phosphorescence (UOP) materials exhibiting persistent emission features can be used in applications such as information encryptions, bioimaging, and display. Until now, the molecular design of UOP materials is mainly focused on intermolecular interactions without consideration to intramolecular interactions. Here, a series of highly twisted molecules exhibit non-radiative decay as low as 1.01 s^{-1} due to the restriction of the excited molecular motions by synergy of intramolecular and intermolecular interactions in the molecular crystals. A unique insight regarding the importance of intramolecular interactions in suppressing non-radiative decay as well as the intermolecular interactions is provided in this contribution. Significantly, two of the phosphors display color-dynamic UOP emissions in a wide range (from pink to white then orange), which exhibit linearly tunable emissions after ceasing of the excitation source. Moreover, owing to the dual ultralong emission feature, a stable white-light persistent emission is realized for the first time in the molecular crystal. These findings provide the opportunity for the development of dynamic luminescence in organic materials.

SUPPORTING INFORMATION

Table of Contents

1. Experimental Procedures	3
2. Results and Discussion	3
2.1 Synthesis route	3
2.2 Photophysical properties.....	5
2.3 Chemical characterization.....	28
References.....	44
Author Contributions.....	44

SUPPORTING INFORMATION

1. Experimental Procedures

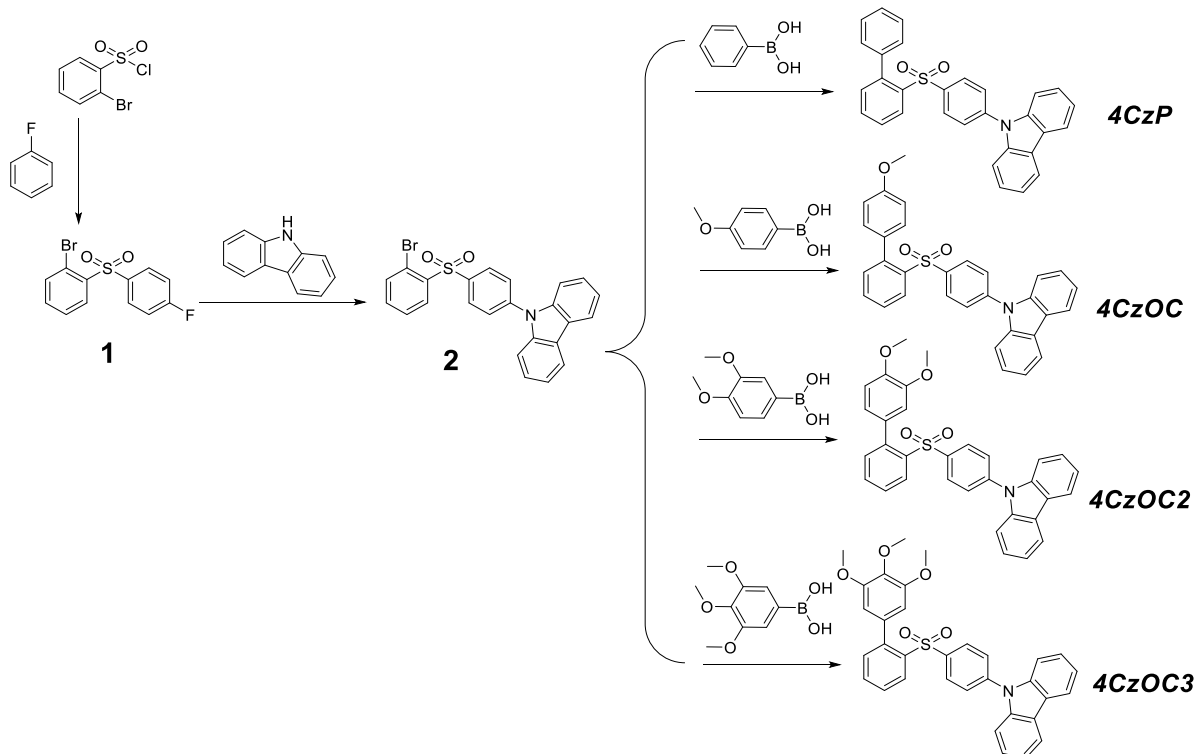
Reagents and Materials: The reagents and solvents were purchased from the commercial sources and without any further purification. 2-bromobenzenesulfonyl chloride, 2-fluorobenzenesulfonyl chloride, carbazole, bromobenzene, and fluorobenzene were purchased from Aladdin company. Phenylboronic acid, 4-methoxyphenylboronic acid, 3,4-dimethoxyphenylboronic acid, and 3,4,5-trimethoxyphenylboronic acid were bought from Soochiral Chemical Science & Technology Company. The solvents dichloride methane, hexane, tetrahydrofuran (THF), and dimethylformamide (DMF) were purchased from Guangzhou chemical reagents factory.

Physical Measurements: ^1H NMR and ^{13}C NMR spectra were performed on a Bruker AVANCE 400 spectrometer in DMSO-d_6 and CDCl_3 , respectively. UV-Visible absorption and photoluminescence spectra of solutions were measured on Hitachi U-3900 and SHIMADZU FR-5301pc, respectively. Photoluminescence profiles, fluorescence lifetime, and phosphorescence lifetime decay curves were obtained on Horiba JY FL-3 spectrometer. Decay curves were obtained on Ocean Optics QE65 Pro and triggered with LED light source (365 nm). Fluorescence and phosphorescence quantum yields were measured on Horiba JY FL-3 spectrometer equipped with a calibrated integrating sphere. Single crystals X-ray diffraction data were collected from Agilent Technologies Gemini A Ultra system with Cu-K α radiation. Ultralong phosphorescent photographs of the crystalline samples were excited by a LED light (365 nm) and obtained with a Canon EOS 550D Camera. The UOP pattern of horse was captured by a Xiaomi 8 mobile phone.

Computational Methods: Time-Dependent Density Functional Theory (TD-DFT) calculations were carried out through Gaussian 09 software at B3LYP/6-31+g* level.^[1] Geometries of these molecules were obtained through the simulation in a cavity of a THF solvent and using the polarizable continuum model for the discussion in THF solutions. Non-covalent interactions (NCI) of intramolecular and intermolecular interactions analysis were carried out by Multiwfn (version 3.5) with reduced density gradient (RDG) and independent gradient model (IGM), respectively.^[2] RDG and IGM analysis were performed with the Gaussian simulations DFT results. The NCI results were plotted via VMD software (version 1.9.3) with appropriate isovalue for visualization.^[3] NTO analysis were carried out with TD-DFT simulations and extracted by the Multiwfn and plotted via GaussView (version 6.0.16) with a isovalue of 0.02. Spin-orbit coupling (SOC) constants were obtained through PySOC software based on the TD-DFT results.^[4] The detailed processing of the simulations can be found in website (<http://sobereva.com/wfnbbs/>). The RDG, IGM, NTO, and SOC were simulated based on the geometries which were extracted from their corresponding single crystals.

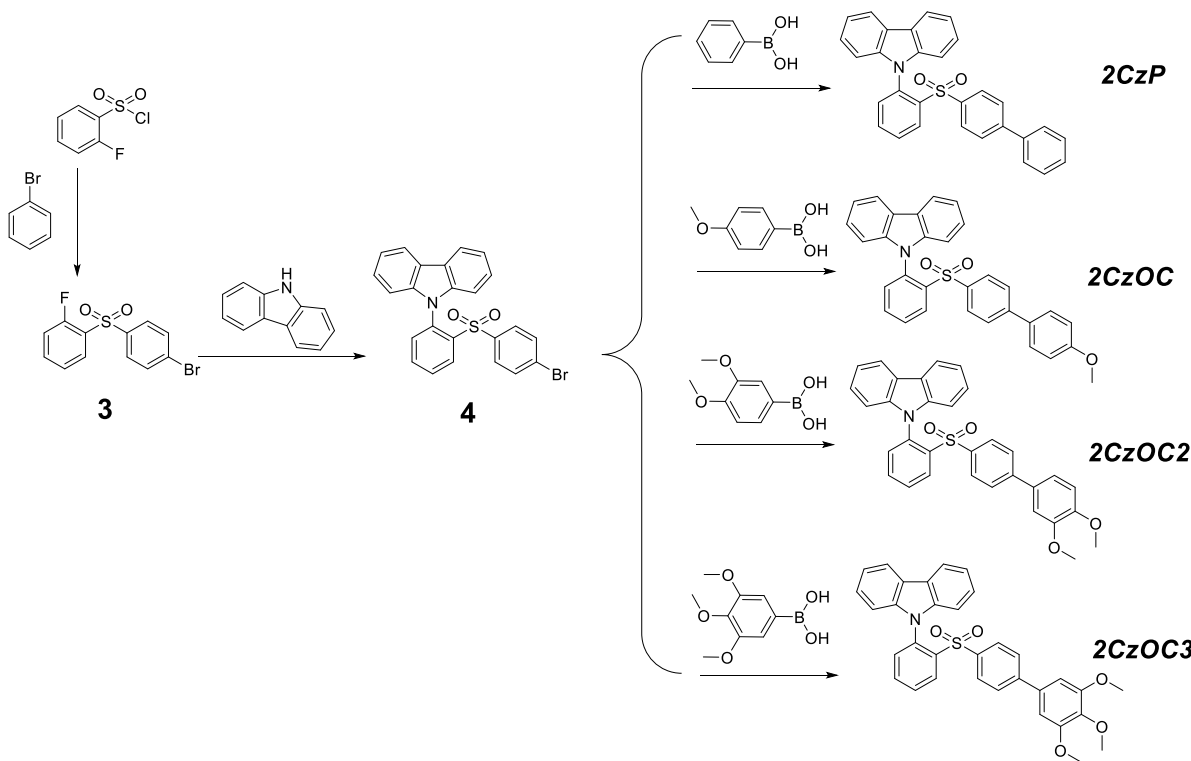
2. Results and Discussion

2.1 Synthesis route



SUPPORTING INFORMATION

Scheme S1. Synthesis route of the *para*-substituents.



Scheme S2. Synthesis route of the *ortho*-substituents.

Synthesis of 9-(4-([1,1'-biphenyl]-2-ylsulfonyl)phenyl)-9H-carbazole (4CzP): the intermediate compounds 1 and 2 were prepared according to the previous work (Scheme S1).^[5] 4CzP was obtained through Suzuki coupling reaction of the 2 and phenylboronic acid using tetrakis(triphenylphosphine)palladium as the catalyst, affording white powder (0.20 g) with a yield of 66.7%. ¹H NMR (DMSO-*d*₆): δ 8.42 (d, 1H), 8.27 (d, 2H), 7.80 (p, 2H), 7.60 (d, 2H), 7.48 (t, 6H), 7.37 (t, 4H), 7.27 (t, 2H), 7.07 (d, 2H). ¹³C NMR (CDCl₃): δ 142.13, 141.66, 140.03, 139.56, 138.85, 138.15, 133.25, 132.76, 130.22, 129.52, 128.55, 127.85, 127.80, 127.58, 126.28, 126.16, 123.88, 120.82, 120.56, 109.51. EI-MS m/z: [m]⁺ calcd for C₃₀H₂₁NO₂S, 459, found 459. HRMS m/z: [m]⁺ calcd for C₃₀H₂₁NO₂S, 459.1293, found 459.1285.

Synthesis of 9-(4-((4'-methoxy-[1,1'-biphenyl]-2-yl)sulfonyl)phenyl)-9H-carbazole (4CzOC): following the similar synthetic method for 4CzP to give 4CzOC (0.39 g, 73.6%) as white solid. ¹H NMR (DMSO-*d*₆): δ 8.39 (d, 1H), 8.25 (d, 2H), 7.75 (d, 2H), 7.60 (d, 2H), 7.51–7.42 (m, 6H), 7.33 (dd, 3H), 6.99 (d, 2H), 6.82 (d, 2H), 3.77 (s, 3H). ¹³C NMR (CDCl₃): δ 159.42, 141.97, 141.66, 140.01, 139.76, 138.91, 133.25, 133.07, 131.47, 130.42, 129.46, 128.60, 127.61, 126.29, 126.06, 123.89, 120.82, 120.56, 113.04, 110.00, 109.56, 55.40. EI-MS m/z: [m]⁺ calcd for C₃₁H₂₃NO₃S, 489, found 489. HRMS m/z: [m]⁺ calcd for C₃₁H₂₃NO₃S, 489.1399, found 489.1392.

Synthesis of 9-(4-((3',4'-dimethoxy-[1,1'-biphenyl]-2-yl)sulfonyl)phenyl)-9H-carbazole (4CzOC2): following the similar synthetic method for 4CzP to give 4CzOC2 (0.20 g, 58.8%) as white solid. ¹H NMR (DMSO-*d*₆): δ 8.39 (d, 1H), 8.24 (d, 2H), 7.81–7.70 (m, 2H), 7.61 (d, 2H), 7.51–7.41 (m, 6H), 7.39–7.28 (m, 3H), 6.89 (d, 1H), 6.67 (dd, 1H), 6.60 (d, 1H), 3.78 (s, 3H), 3.52 (s, 3H). ¹³C NMR (CDCl₃): δ 148.85, 147.83, 141.97, 141.76, 139.92, 139.71, 138.81, 133.26, 133.00, 130.65, 129.55, 128.70, 127.71, 126.29, 125.86, 123.93, 122.58, 120.89, 120.54, 114.16, 110.34, 110.00, 109.54, 56.05, 55.92. EI-MS m/z: [m]⁺ calcd for C₃₂H₂₅NO₄S, 519, found 519. HRMS m/z: [m]⁺ calcd for C₃₂H₂₅NO₄S, 519.1504, found 519.1495.

Synthesis of 9-(4-((3',4'-dimethoxy-[1,1'-biphenyl]-2-yl)sulfonyl)phenyl)-9H-carbazole (4CzOC3): following the similar synthetic method for 4CzP to give 4CzOC3 (0.35 g, 72.9%) as white solid. ¹H NMR (500 MHz, DMSO-*d*₆) δ 8.43 (dd, 1H), 8.26 (d, 2H), 7.80 (td, 2H), 7.66 (d, 2H), 7.52 (d, 2H), 7.49–7.41 (m, 5H), 7.34 (ddd, 2H), 6.41 (s, 2H), 3.75 (s, 3H), 3.62 (s, 6H). ¹³C NMR (126 MHz, CDCl₃) δ 152.28, 141.97, 141.93, 139.83, 139.67, 138.66, 137.85, 133.28, 133.18, 132.55, 129.61, 128.69, 127.90, 126.34, 125.72, 123.95, 120.96, 120.47, 109.65, 107.86, 61.14, 56.15. EI-MS m/z: [m]⁺ calcd for C₃₃H₂₇NO₅S, 549, found 549. HRMS m/z: [m]⁺ calcd for C₃₃H₂₇NO₅S, 549.1610, found 549.1603.

Synthesis of 9-(2-([1,1'-biphenyl]-4-ylsulfonyl)phenyl)-9H-carbazole (2CzP): following the similar synthetic method (Scheme S2) for 4CzP to give 2CzP. (0.38 g, 76.0%). ¹H NMR (500 MHz, DMSO-*d*₆) δ 8.55 (dd, 1H), 8.12 (d, 2H), 8.04–7.88 (m, 2H), 7.50–7.34 (m, 6H), 7.21–6.93 (m, 8H), 6.43 (d, 2H). ¹³C NMR (CDCl₃) δ 145.90, 142.61, 142.24, 139.31, 137.59, 136.30, 135.25, 132.68, 129.99, 129.87, 128.77, 128.29, 128.15, 127.42, 126.99, 125.75, 123.32, 120.13, 119.74, 110.55. EI-MS m/z: [m]⁺ calcd for C₃₀H₂₁NO₂S, 459, found 459. HRMS m/z: [m]⁺ calcd for C₃₀H₂₁NO₂S, 459.1293, found 459.1284.

Synthesis of 9-(2-((4'-methoxy-[1,1'-biphenyl]-4-yl)sulfonyl)phenyl)-9H-carbazole (2CzOC): the intermediate compounds 3 and 4 were prepared according to the previous work (Scheme S2).^[5] Following the similar synthetic method for 2CzP to give 2CzOC (0.37 g,

SUPPORTING INFORMATION

69.8%) as white solid. ^1H NMR (500 MHz, DMSO- d_6) δ 8.54 (dd, 1H), 8.12 (d, 2H), 7.95 (qd, 2H), 7.42–7.33 (m, 3H), 7.11 (t, 4H), 7.07–6.98 (m, 4H), 6.95 (d, 2H), 6.42 (d, 2H), 3.84–3.71 (m, 3H). ^{13}C NMR (126 MHz, CDCl₃) δ 159.93, 145.49, 142.71, 142.25, 136.84, 136.28, 135.16, 132.66, 131.70, 129.97, 129.83, 128.53, 128.16, 126.41, 125.73, 123.31, 120.08, 119.70, 114.22, 110.57, 55.38. EI-MS m/z: [m]⁺ calcd for C31H23NO3S, 489, found 489. HRMS m/z: [m]⁺ calcd for C31H23NO3S, 489.1399, found 489.1391.

Synthesis of 9-(2-((3',4'-dimethoxy-[1,1'-biphenyl]-4-yl)sulfonyl)phenyl)-9H-carbazole (2CzOC2): following the similar synthetic method for 2CzP to give 2CzOC2 (0.41 g, 73.2%) as white solid. ^1H NMR (500 MHz, DMSO- d_6) δ 8.58–8.51 (m, 1H), 8.17–8.09 (m, 2H), 8.01–7.91 (m, 2H), 7.37 (dd, 1H), 7.14 (dd, 4H), 7.09–6.91 (m, 7H), 6.44 (d, 2H), 3.84 (s, 3H), 3.79 (s, 3H). ^{13}C NMR (126 MHz, CDCl₃) δ 149.45, 149.13, 145.73, 142.65, 142.30, 137.01, 136.29, 135.21, 132.65, 132.16, 129.97, 129.86, 128.17, 126.58, 125.75, 123.33, 120.06, 119.99, 119.70, 111.34, 110.62, 110.52, 56.02, 56.00. EI-MS m/z: [m]⁺ calcd for C32H25NO4S, 519, found 519. HRMS m/z: [m]⁺ calcd for C32H25NO4S, 519.1504, found 519.1496.

Synthesis of 9-(2-((3',4',5'-trimethoxy-[1,1'-biphenyl]-4-yl)sulfonyl)phenyl)-9H-carbazole (2CzOC3): following the similar synthetic method for 2CzP to give 2CzOC3 (0.40 g, 67.8%) as white solid. ^1H NMR (500 MHz, DMSO- d_6) δ 8.55 (dd, 1H), 8.14 (d, 2H), 8.01–7.91 (m, 2H), 7.35 (dd, 1H), 7.21–7.12 (m, 4H), 7.08 (dd, 2H), 6.97 (d, 2H), 6.64 (s, 2H), 6.43 (d, 2H), 3.85 (s, 6H), 3.68 (s, 3H). ^{13}C NMR (126 MHz, CDCl₃) δ 153.43, 146.04, 142.54, 142.33, 138.42, 137.56, 136.31, 135.29, 135.21, 132.65, 129.98, 129.89, 128.17, 126.91, 125.76, 123.35, 120.05, 119.73, 110.65, 104.76, 60.99, 56.27. EI-MS m/z: [m]⁺ calcd for C33H27NO5S, 549, found 549. HRMS m/z: [m]⁺ calcd for C33H27NO5S, 549.1610, found 549.1602.

2.2 Photophysical properties

Photophysical properties in solutions. With the intention to investigate the monomeric molecular photophysical properties, the absorption and photoluminescence (PL) spectra of the 8 molecules were recorded in dilute THF solution ($\sim 10^{-5}$ M, Figure 2). Intriguingly, the UV-Vis absorption profiles of *para*-substituents (4CzP, 4CzOC, 4CzOC2, 4CzOC3) show nearly identical bands but the PL spectra display significant differences. The opposite phenomenon is observed in the *ortho*-substituents (2CzP, 2CzOC, 2CzOC2, 2CzOC3), wherein, noticeably, the UV-Vis absorption profiles differ from each other, but the PL spectra are identical. As shown in Figure 2, the maximum emission wavelength (λ_{max}) of the structureless PL in the *ortho*-substituents is red-shifted to ca. 449 nm, comparing to the $\lambda_{\text{max}} = 404$ nm (4CzP), 398 nm (4CzOC), 419 nm (4CzOC2) and 402 nm (4CzOC3) of the *para*-substituents. Additionally, the lifetime of the *ortho*-substituents (11 ns) is longer than that of the *para*-substituents (6.5 ns). These results indicate that the *ortho*-substituents possess stronger intramolecular charge transfer (ICT) properties.^[6] The mechanism of the ICT properties occurring in *para*- and *ortho*-substituents can be further studied by considering the geometries of the 8 molecules that have been simulated in a cavity of THF solvent with the polarizable continuum model (PCM). As shown in Figure S1, the 8 molecules exhibit folded conformations with intramolecular steric hindrance. In *ortho*-substituents, the carbazole moieties are sterically “locked” in nearly perpendicular orientation (over 80°) with the diphenylsulphone moieties ($\theta_{\text{A-B}}$ represents the dihedral angle) (Figure S2a). Therefore, the frontier orbitals of HOMOs and LUMOs are separately localized on donors (carbazoles) and acceptors (diphenylsulphones) due to the highly twisted linkage,^[7] which implies the red-shifted emission and longer lifetimes in THF solutions for *ortho*-substituents (Figure S3).^[8] As depicted in Figure S4, the HOMOs in *para*-substituents are primarily contributed by the phenyl-carbazole moieties for the small angles of $\theta_{\text{A-B}}$ (Figure S2b). Intriguingly, the angle of phenyl rings C and D ($\theta_{\text{C-D}}$) in 4CzOC2 is much smaller than that in 4CzP, 4CzOC, and 4CzOC3. As reported before, coplanar connectivity can afford an enhancement of the conjugation between two phenyl rings.^[9] Thus, the dimethoxybenzene moiety in 4CzOC2 also acts as an electron-donating moiety as well as the phenyl-carbazole, which can be evidenced by the theoretical calculations showing the HOMO localizes on the dimethoxybenzene and phenyl-carbazole simultaneously (Figure S4). This indicates that the enhanced electron-donating feature is responsible for the slightly red-shifted emission of 4CzOC2 in THF solutions among the *para*-substituents. The simulated geometries and the photophysical characterization for isolate states indicate that the intramolecular dihedral angles ($\theta_{\text{A-B}}$ and $\theta_{\text{C-D}}$) in these compounds have a striking influence on the ICT state. As reported previously, the ICT state can act as an intermediate state to boost the ISC process that results in phosphorescence under suitable conditions.^[10]

The X-ray crystal structure of compounds. Single crystals were obtained through slow evaporation of a mixed solvents (CCDC numbers of 4CzP, 4CzOC, 4CzOC2, 4CzOC3, 2CzP, 2CzOC, 2CzOC2 and 2CzOC3 are 1970403, 1970404, 1970405, 1970406, 1970408, 1970407, 1970409 and 1970410, respectively. These data can be obtained free of charge from The Cambridge Crystallographic Data Centre via www.ccdc.cam.ac.uk/data_request/cif.)

SUPPORTING INFORMATION

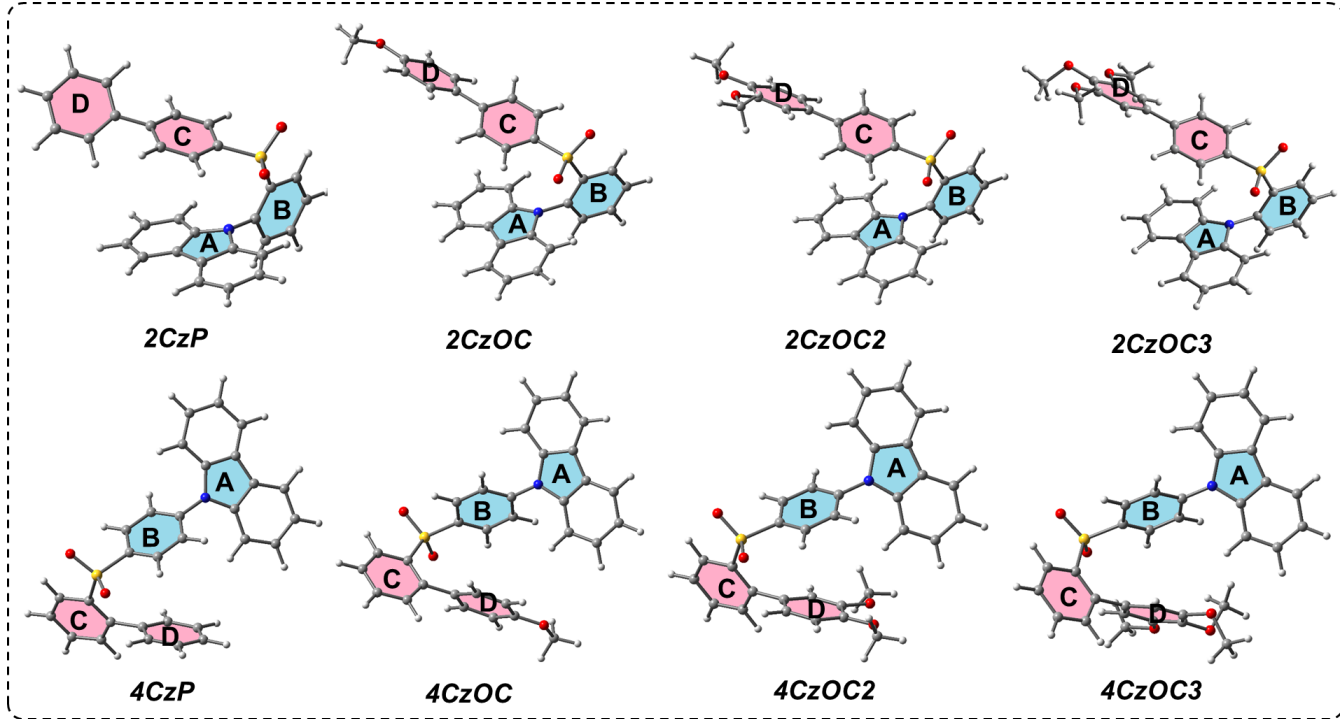


Figure S1. The optimized geometries of the 8 molecules in a cavity of THF solvent with polarizable continuum model. θ_{A-B} represents the dihedral angle between the carbazole unit and diphenylsulphone unit, θ_{C-D} represents the dihedral angle between the phenyl ring and diphenylsulphone unit.

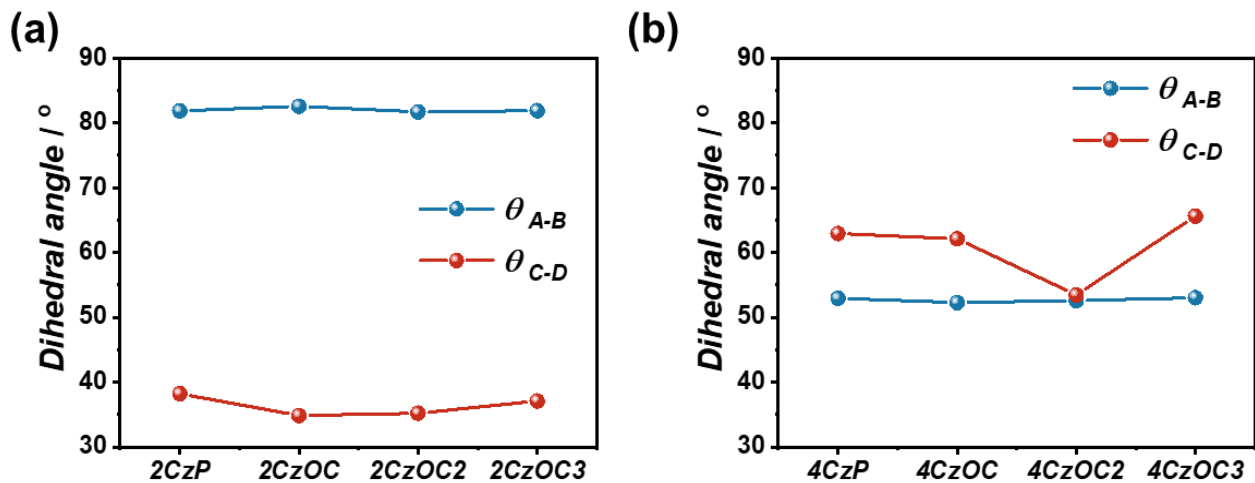


Figure S2. Dihedral angles in the optimized geometries of (a) the *ortho*-substituents and (b) *para*-substituents in a cavity of THF solvent with polarizable continuum model.

SUPPORTING INFORMATION

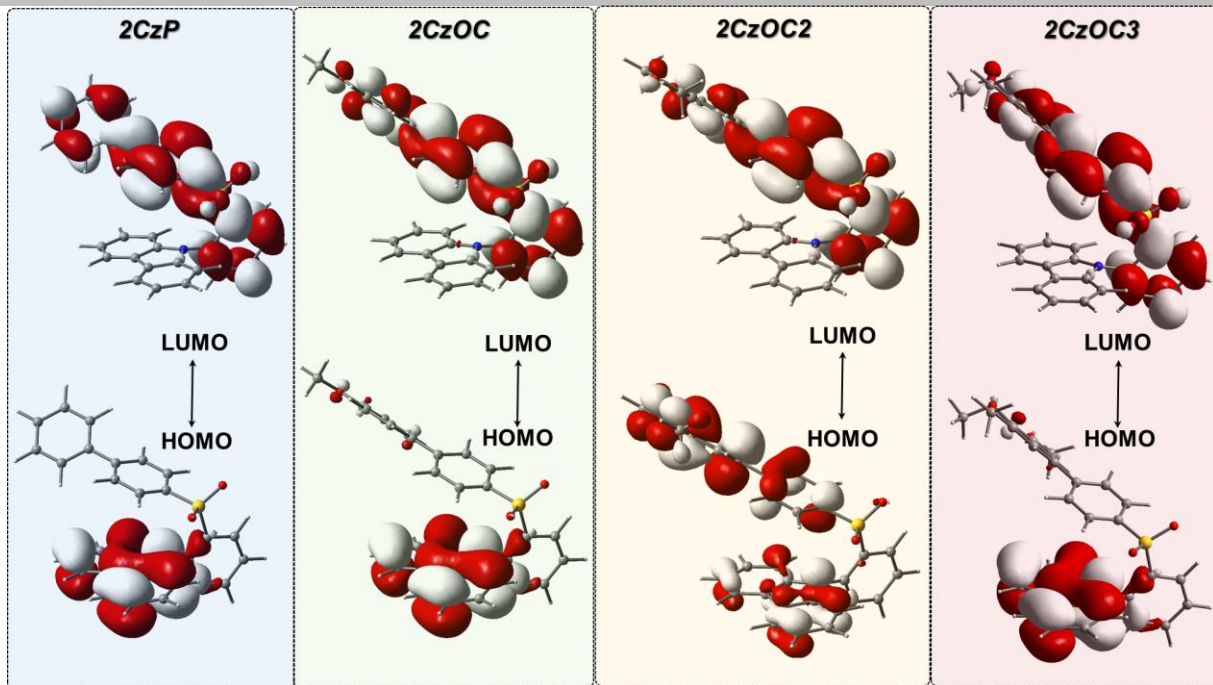


Figure S3. HOMOs and LUMOs of the *ortho*-substituents in THF solutions (isovalue = 0.02).

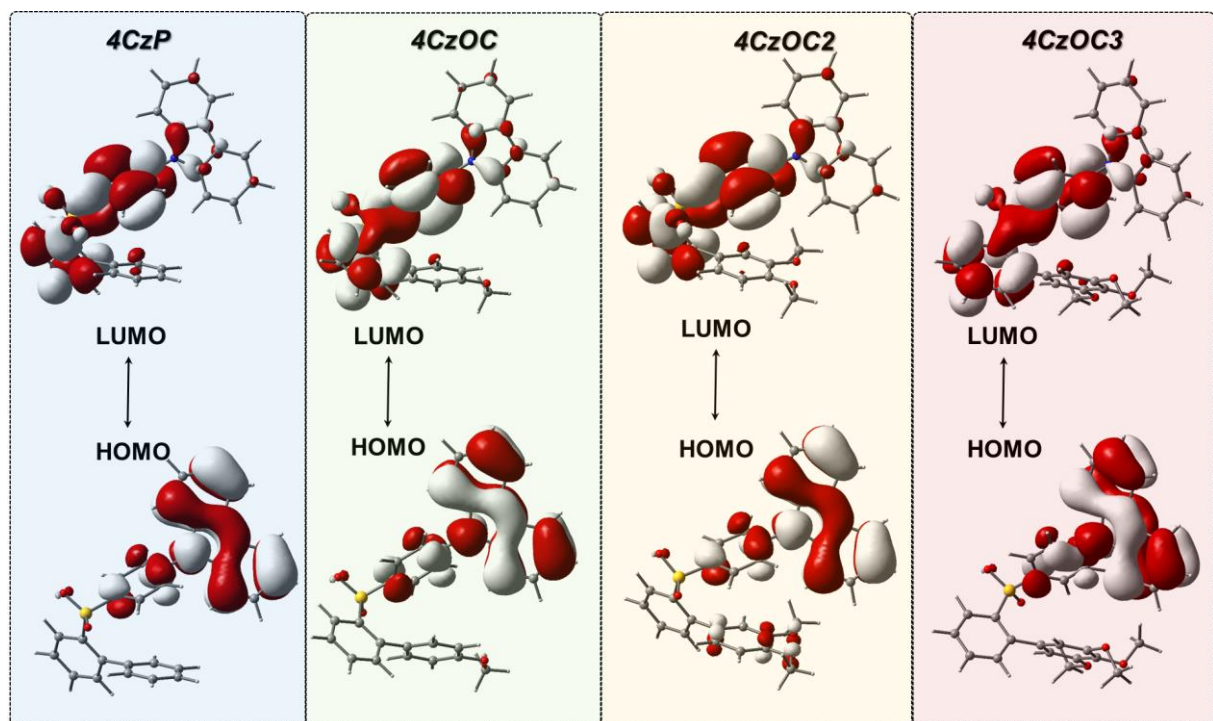


Figure S4. HOMOs and LUMOs of the *para*-substituents in THF solutions (isovalue = 0.02).

SUPPORTING INFORMATION

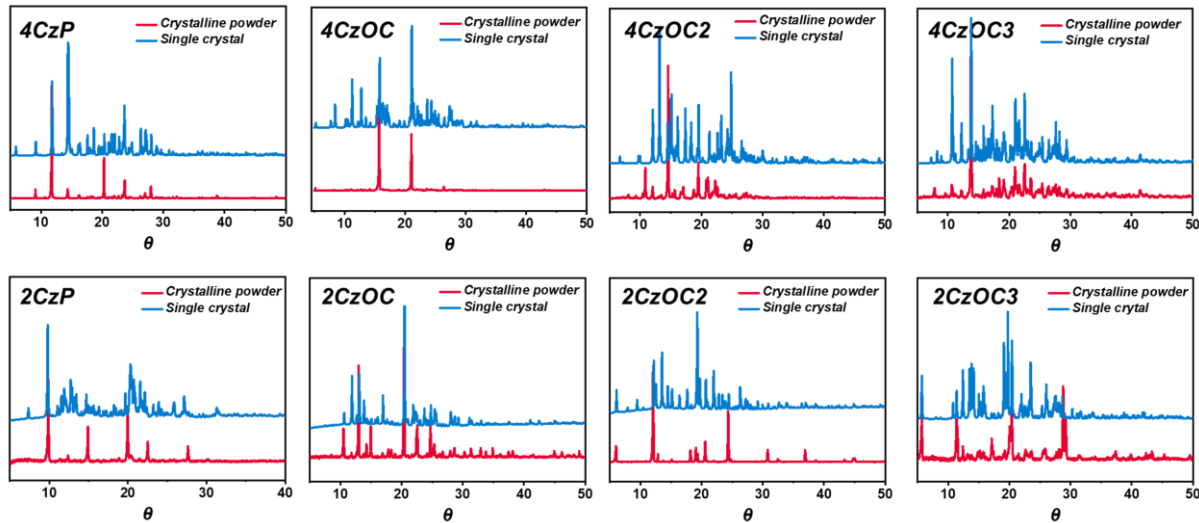


Figure S5. Powder XRD of the crystalline powders and single crystals (blue lines were obtained through simulation).

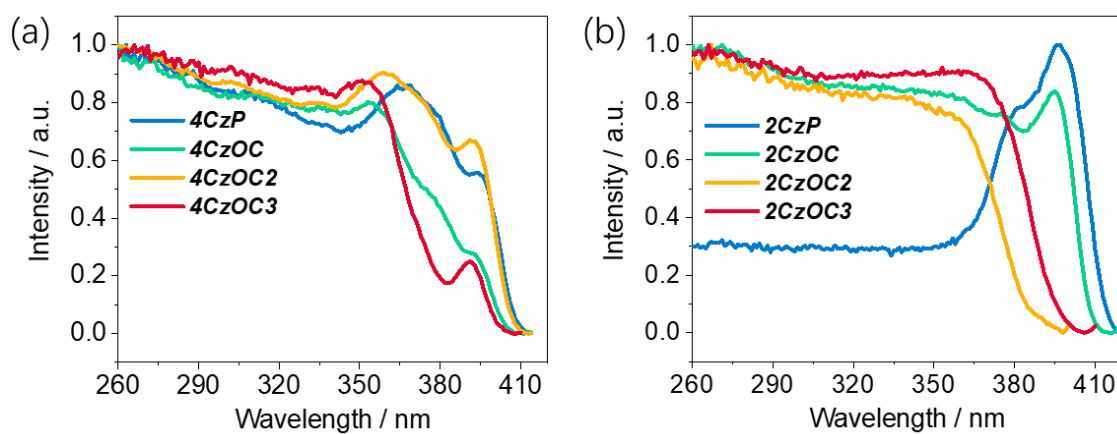


Figure S6. Excitation spectra of the (a) *para*- and (b) *ortho*-substituents.

SUPPORTING INFORMATION

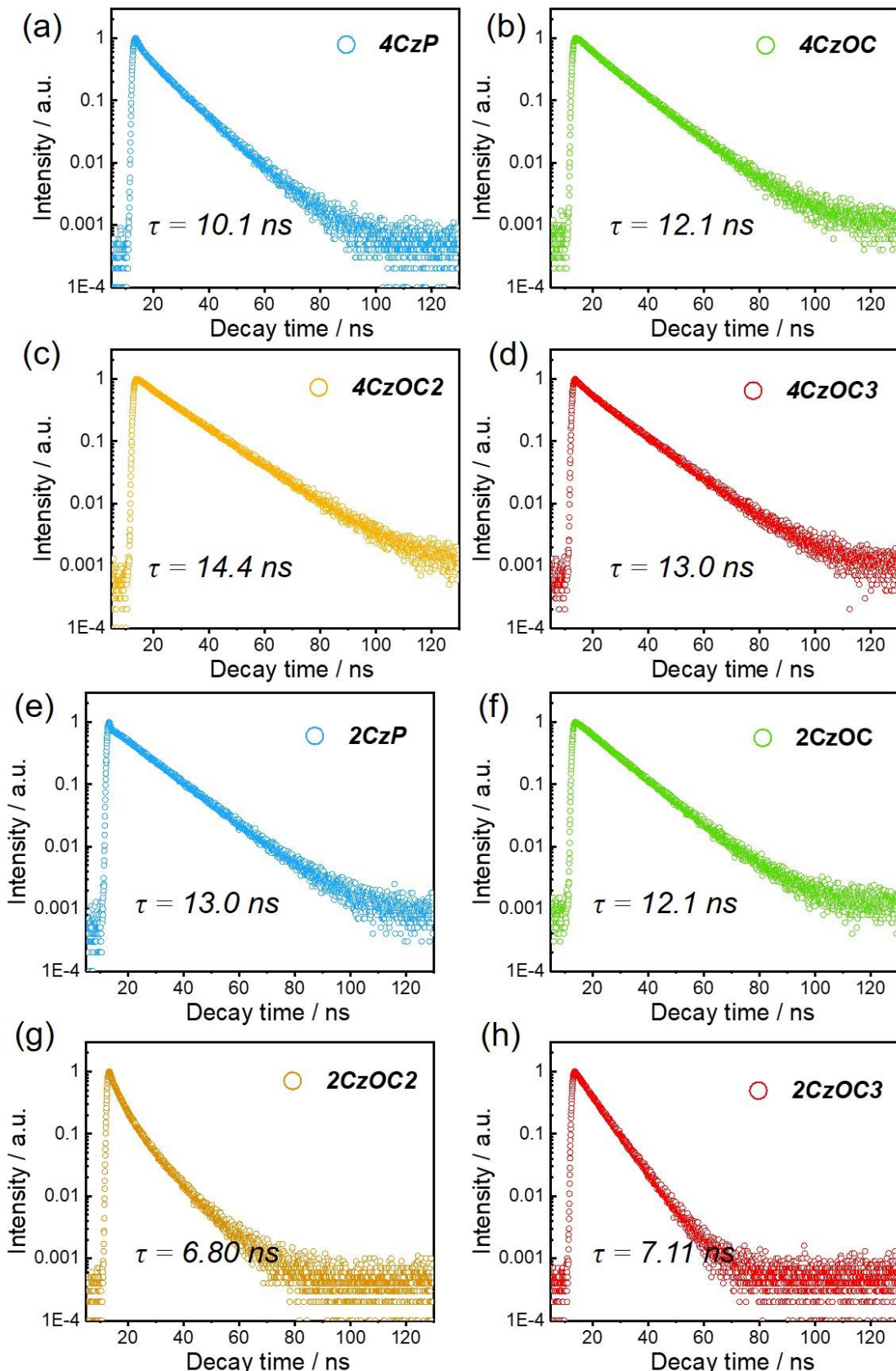


Figure S7. Fluorescence decay curves and lifetimes of the *para*-substituents collected at (a) 427 nm for 4CzP; (b) 426 nm for 4CzOC; (c) 425 nm for 4CzOC2; (d) 427 nm for 4CzOC3. (e) 429 nm for 2CzP; (f) 426 nm for 2CzOC; (g) 417 nm for 2CzOC2; (h) 417 nm for 2CzOC3.

SUPPORTING INFORMATION

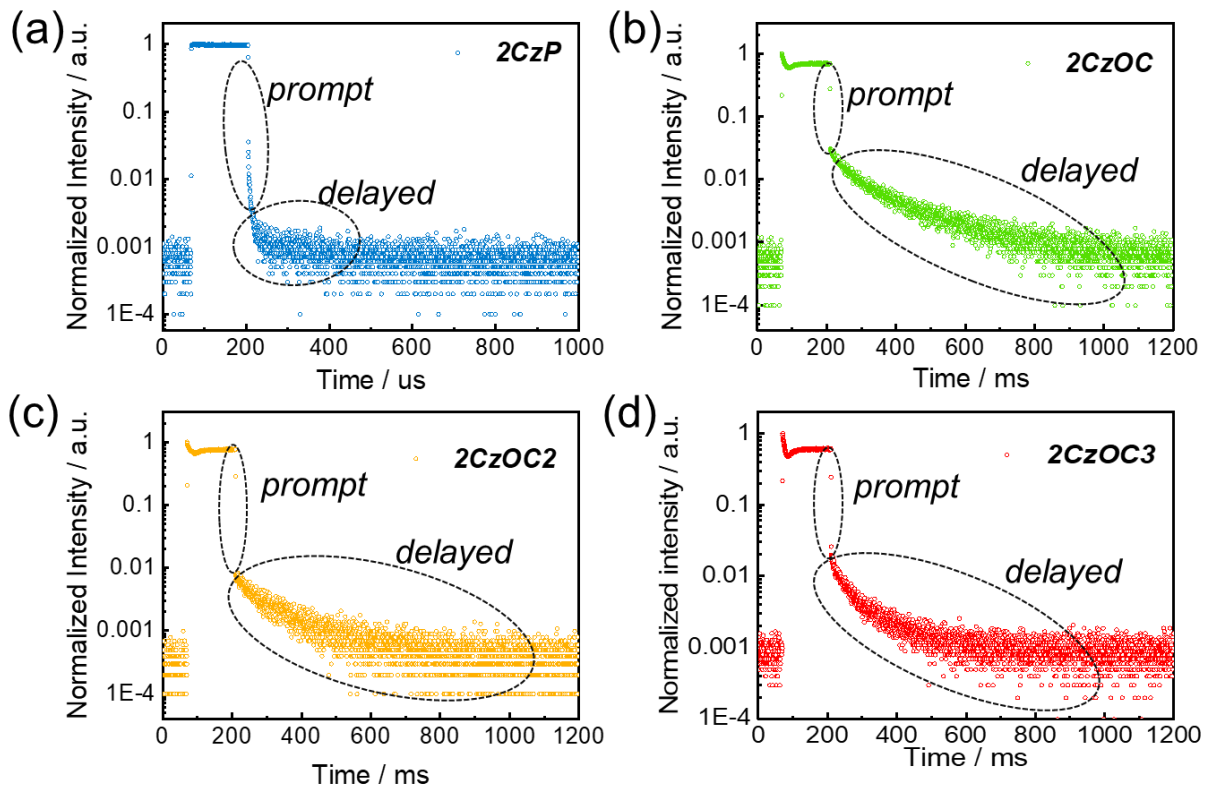


Figure S8. Decay curves of the *ortho*-substituents collected at (a) 429 nm for 2CzP; (b) 426 nm for 2CzOC; (c) 417 nm for 2CzOC2; (d) 417 nm for 2CzOC3.

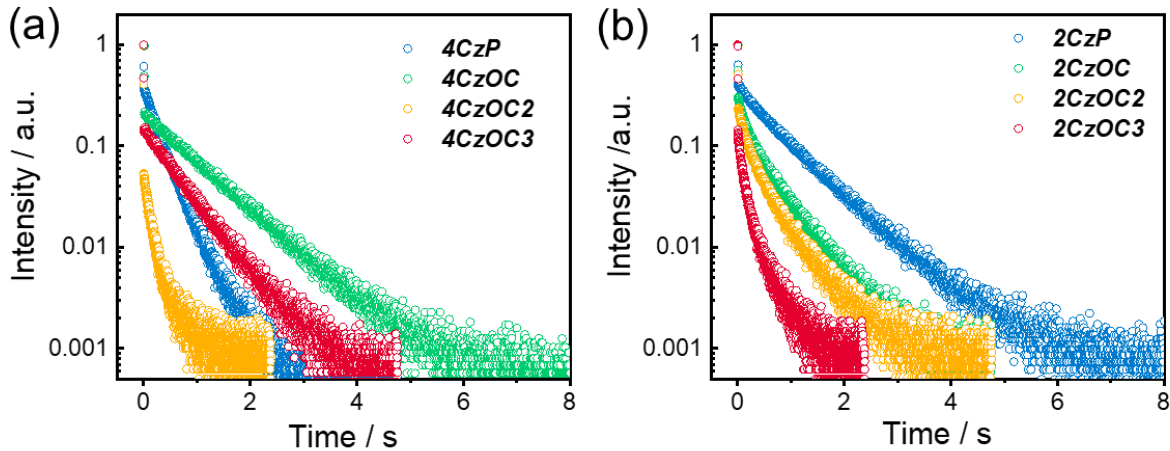


Figure S9. Phosphorescence decay curves of the (a) *para*-substituents (553 nm for 4CzP, 545 nm for 4CzOC, 545 nm for 4CzOC2 and 548 nm for 4CzOC3) and (b) *ortho*-substituents (550 nm for 2CzP, 549 nm for 2CzOC, 545 nm for 2CzOC2 and 542 nm for 2CzOC3) under ambient conditions.

SUPPORTING INFORMATION

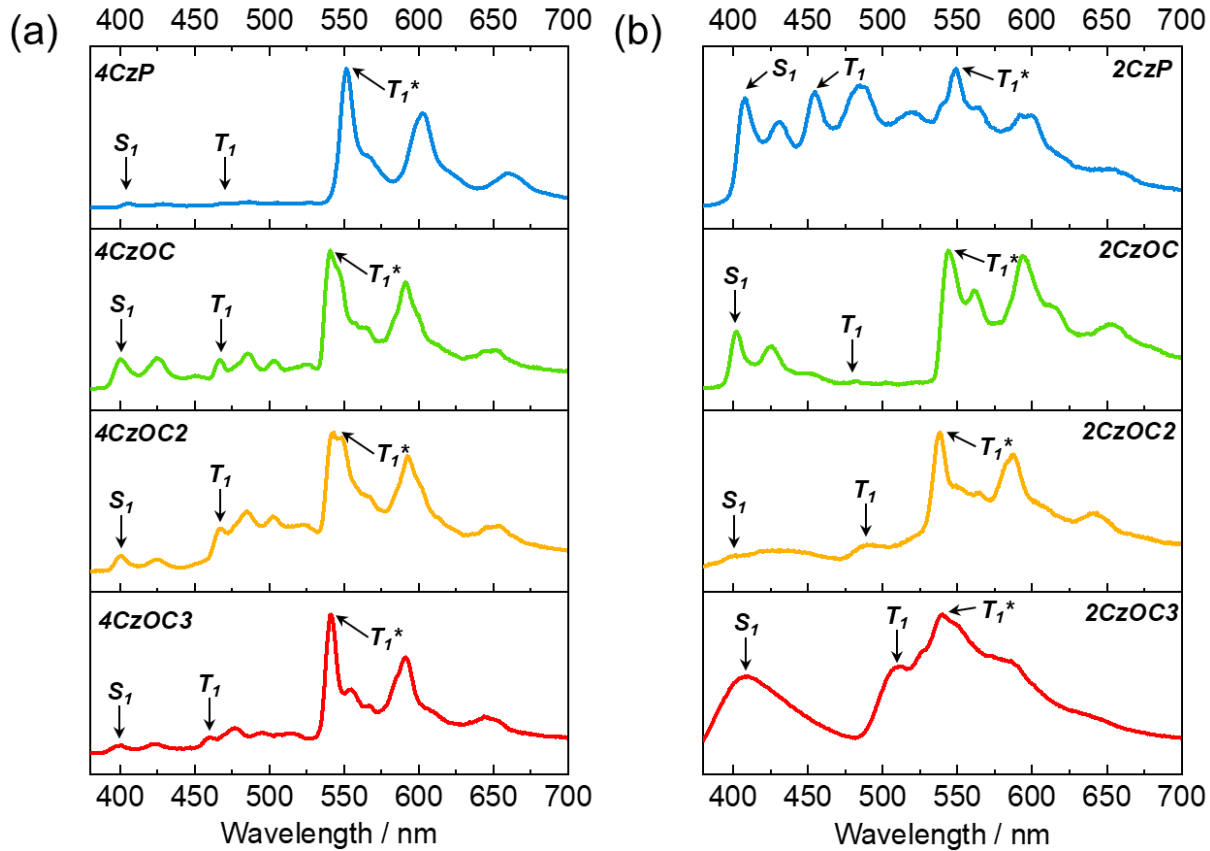


Figure S10. Normalized delayed spectra (delayed time = 8 ms) of (a) *para*-substituents and (b) *ortho*-substituents at 77 K. S₁ and T₁ represent the lowest excited singlet state and the lowest triplet state of isolated molecule. T₁* represents the lowest triplet state of coupling molecules.

Table S1. Photophysical parameters of the *para*- and *ortho*-substituents.

Sample	τ_F/ns	Φ_F	k_F/s^{-1}	τ_P/s	Φ_{TTA}	Φ_P	k_P/s^{-1}	$k_{\text{nr}}/\text{s}^{-1}$	$k_{\text{isc}}/\text{s}^{-1}$
4CzP	10.1	34.65%	3.43×10^7	0.324	0.13%	5.30%	1.64×10^{-1}	2.91	5.51×10^6
4CzOC	12.1	51.68%	4.27×10^7	0.945	0.56%	3.05%	3.23×10^{-2}	1.01	3.45×10^6
4CzOC2	14.4	53.92%	3.74×10^7	0.604	0.02%	0.49%	8.11×10^{-3}	1.65	3.71×10^5
4CzOC3	13.0	23.69%	1.82×10^7	0.625	0.003%	0.08%	1.28×10^{-3}	1.60	6.66×10^4
2CzP	13.0	10.23%	7.86×10^6	0.604	0.12%	1.09%	1.80×10^{-2}	1.63	1.03×10^6
2CzOC	12.1	23.15%	1.91×10^7	0.510	3.58%	0.94%	1.84×10^{-2}	1.80	6.70×10^6
2CzOC2	6.80	13.90%	2.04×10^7	0.401	0.72%	0.55%	1.37×10^{-2}	2.44	2.94×10^6
2CzOC3	7.11	27.22%	3.83×10^7	0.240	0.41%	0.19%	7.92×10^{-3}	4.12	1.41×10^6

τ_F : fluorescence lifetime; Φ_F : fluorescence quantum efficiency; k_F : rate constant of fluorescence; τ_P : phosphorescence lifetime; Φ_P : phosphorescence quantum efficiency; k_P : rate constant of phosphorescence; k_{nr} : rate constant of non-radiative decay of T₁; k_{isc} : rate constant of intersystem crossing from singlet to triplet states. $k_F = \Phi_F/\tau_F$; $k_P = \Phi_P/\tau_P$; $k_{\text{nr}} = (1 - 2\Phi_{\text{TTA}} - \Phi_P)/\tau_P$; $k_{\text{isc}} \approx (2\Phi_{\text{TTA}} + \Phi_P)/\tau_F$. The Φ_{TTA} was obtained through the integral of delayed spectrum.

SUPPORTING INFORMATION

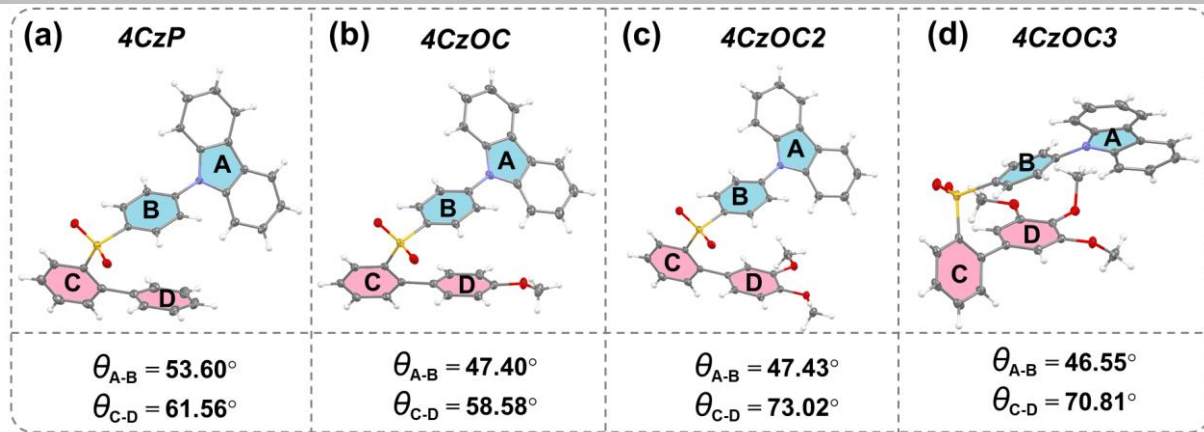


Figure S11. Dihedral angles of the geometries in the single crystals of the *para*-substituents.

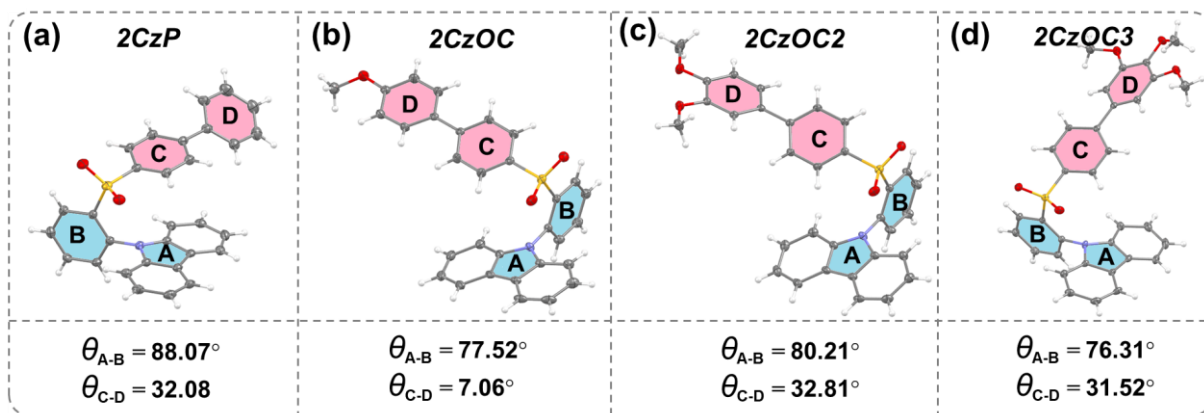


Figure S12. Dihedral angles of the geometries in the single crystals of the *ortho*-substituents.

SUPPORTING INFORMATION

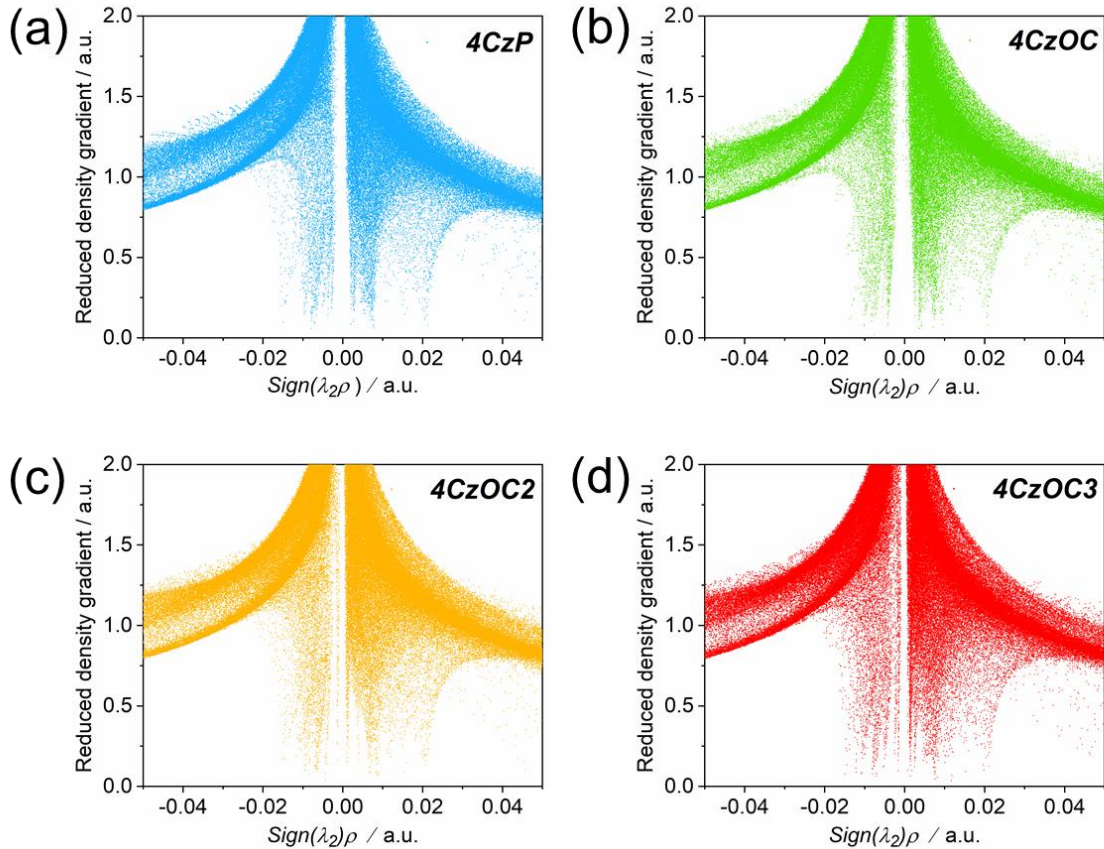


Figure S13. Intramolecular interaction plots (isovalue = 0.5) in RDG models of (a) 4CzP; (b) 4CzOC; (c) 4CzOC2; (d) 4CzOC3.

SUPPORTING INFORMATION

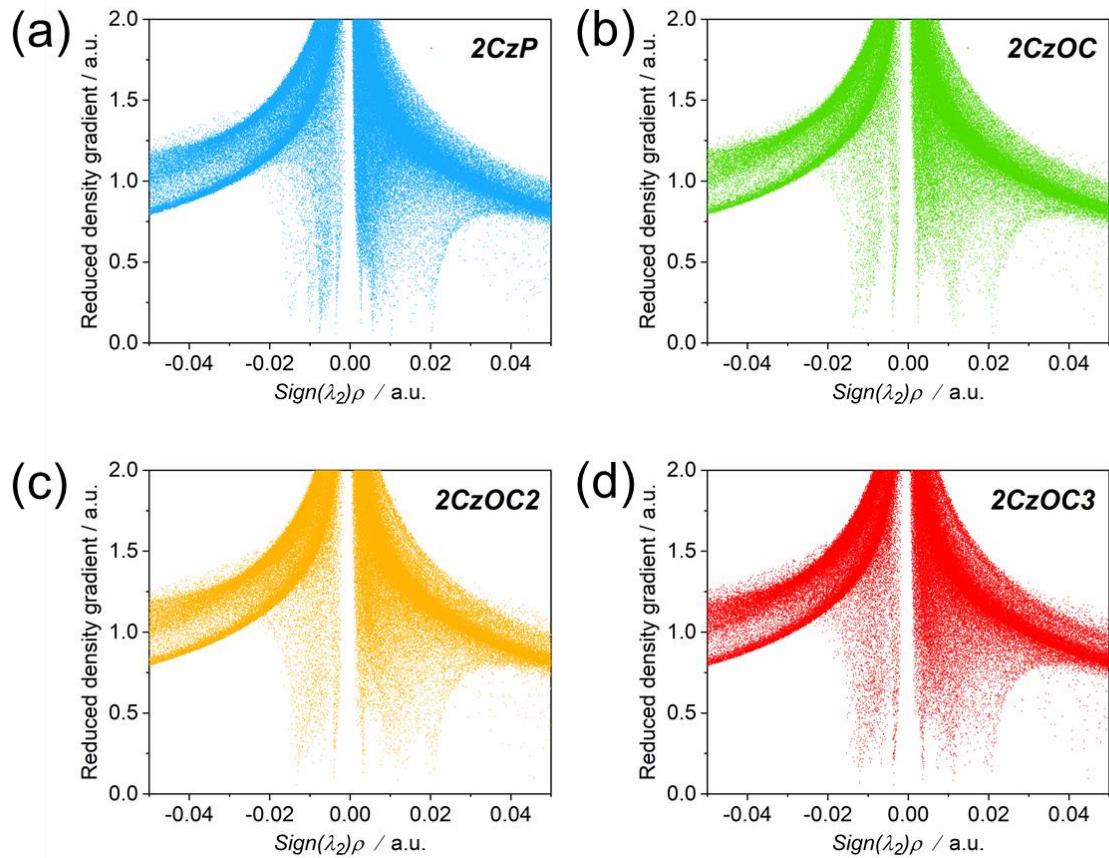


Figure S14. Intramolecular interaction plots (isovalue = 0.5) in RDG models of (a) 2CzP; (b) 2CzOC; (c) 2CzOC2; (d) 2CzOC3.

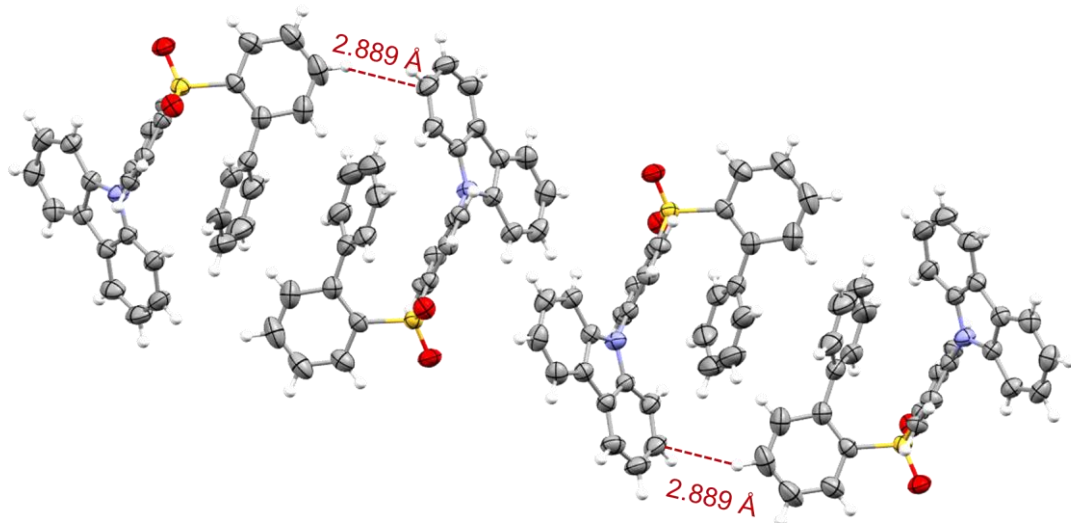


Figure S15. Intermolecular interactions in single crystal (unit cell) of 4CzP.

SUPPORTING INFORMATION

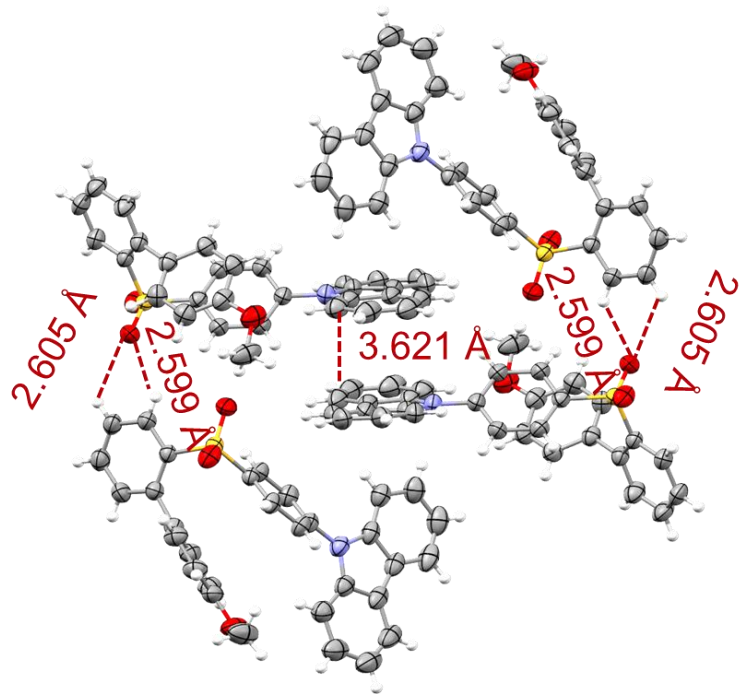


Figure S16. Intermolecular interactions in single crystal (unit cell) of 4CzOC.

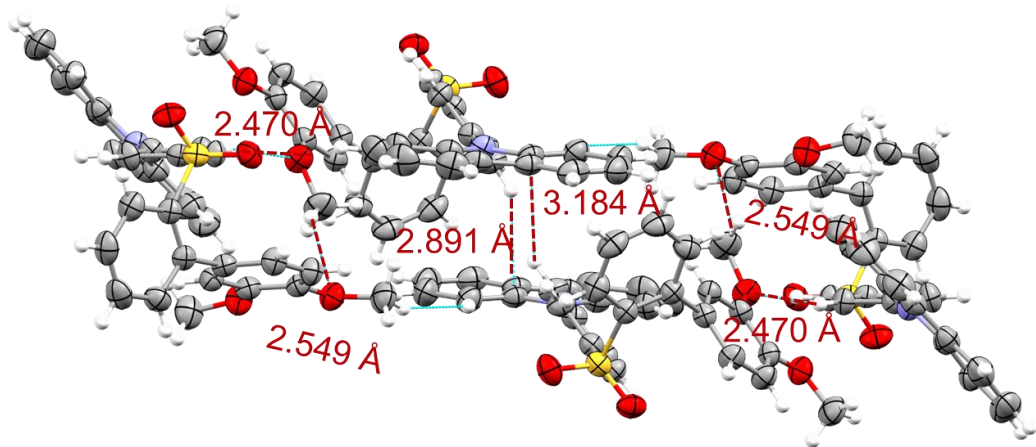


Figure S17. Intermolecular interactions in single crystal (unit cell) of 4CzOC2.

SUPPORTING INFORMATION

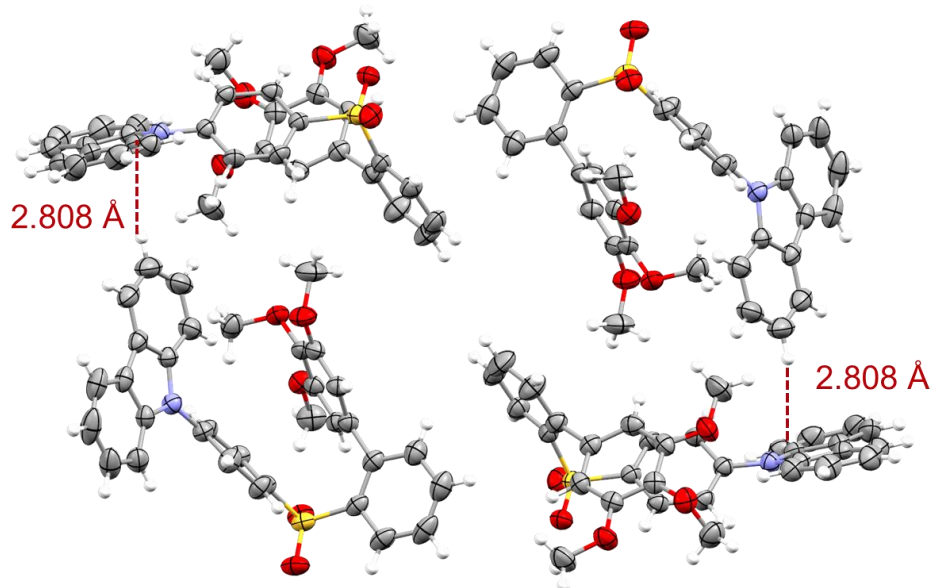


Figure S18. Intermolecular interactions in single crystal (unit cell) of 4CzOC3.

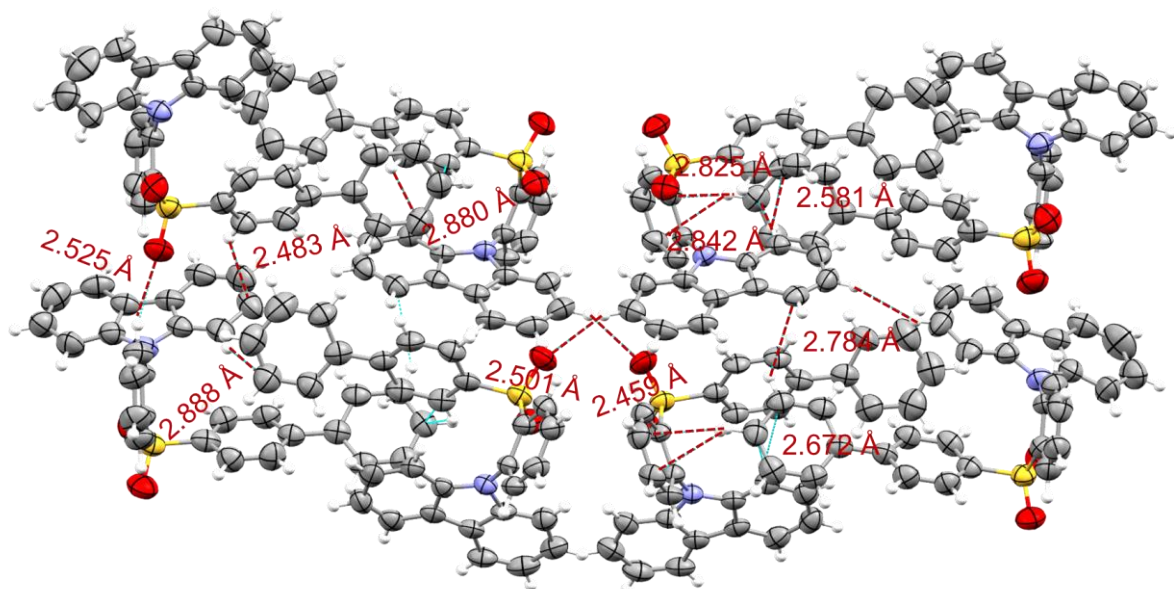


Figure S19. Intermolecular interactions in single crystal (unit cell) of 2CzP.

SUPPORTING INFORMATION

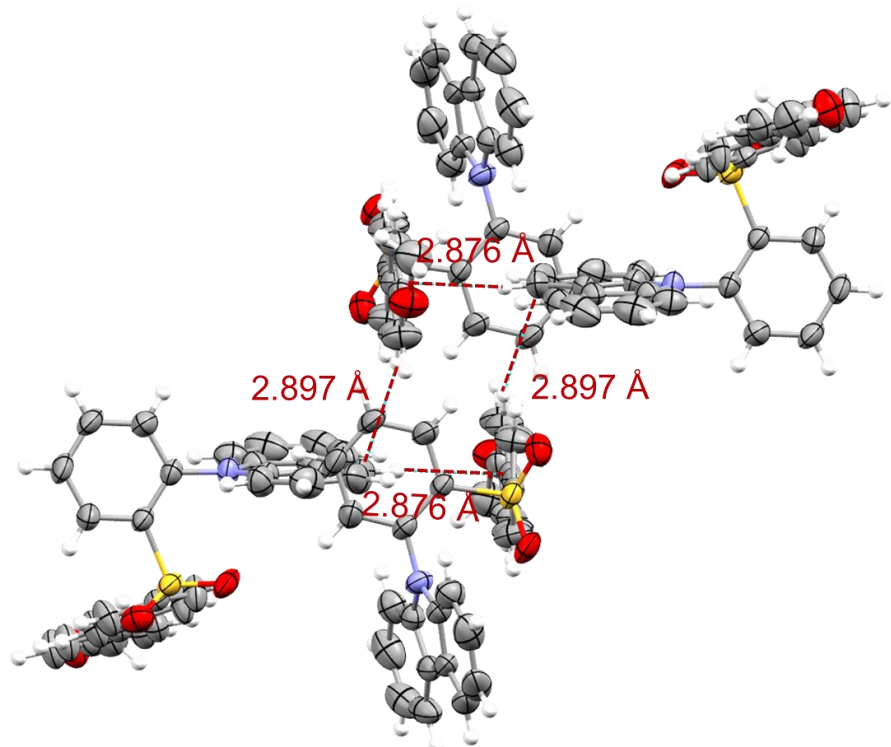


Figure S20. Intermolecular interactions in single crystal (unit cell) of 2CzOC.

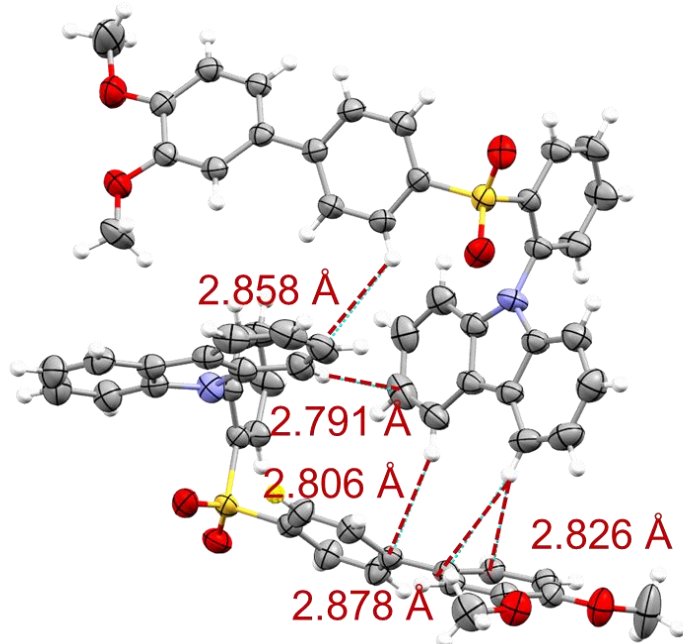


Figure S21. Intermolecular interactions in single crystal (unit cell) of 2CzOC2.

SUPPORTING INFORMATION

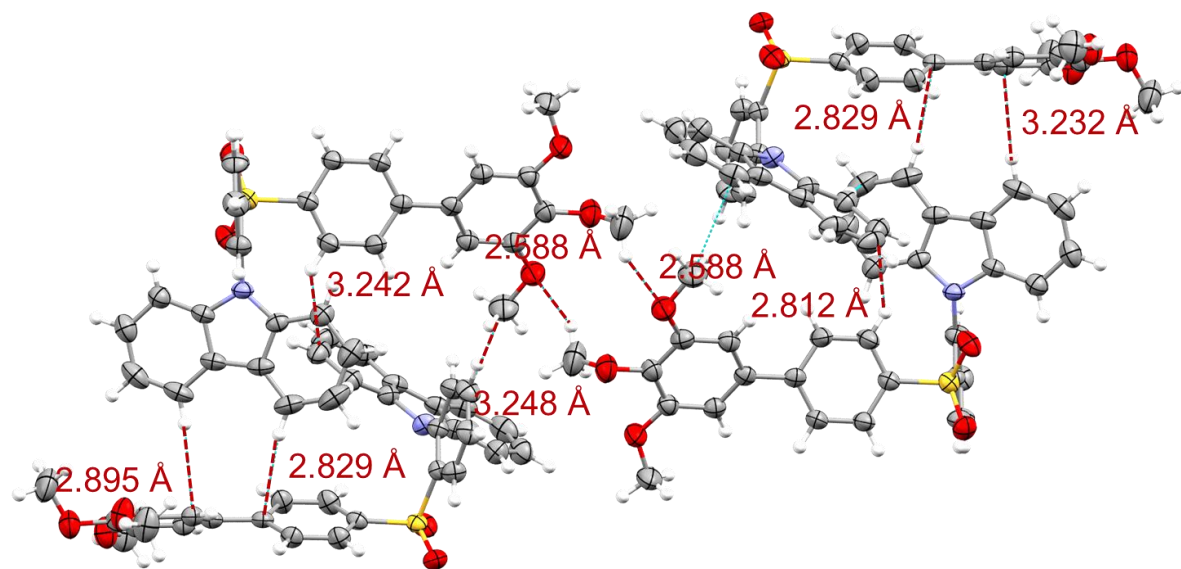


Figure S22. Intermolecular interactions in single crystal (unit cell) of 2CzOC3.

SUPPORTING INFORMATION

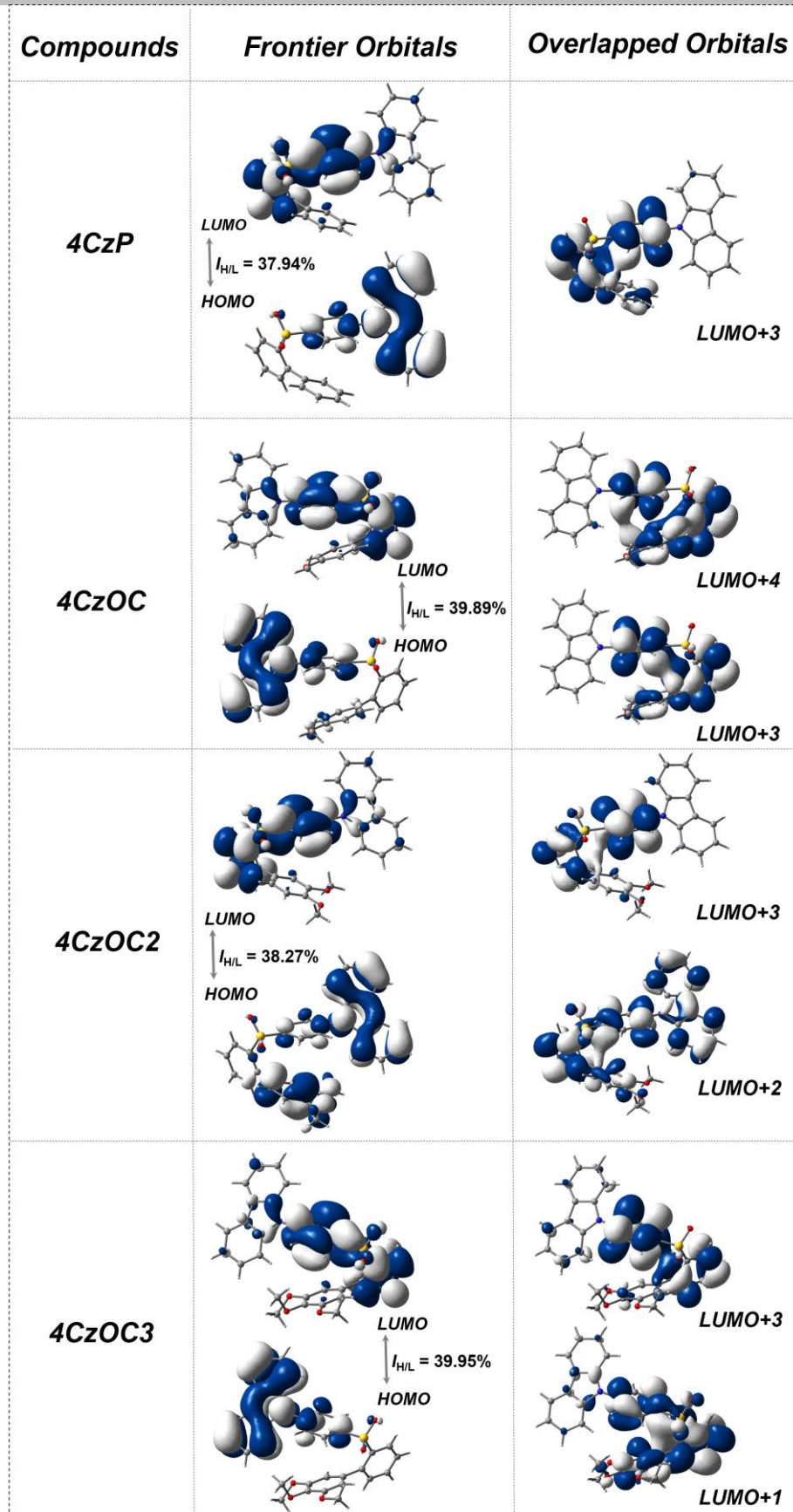


Figure S23. Frontier orbitals and the overlapped orbitals in *para*-substituents (isovalue = 0.02).

SUPPORTING INFORMATION

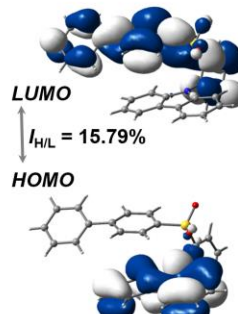
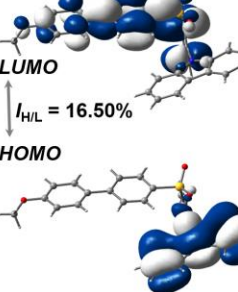
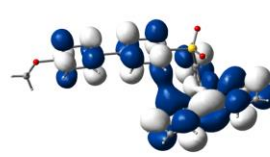
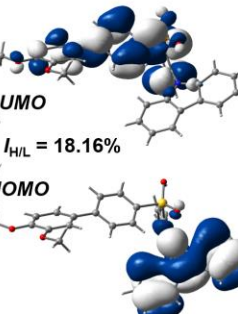
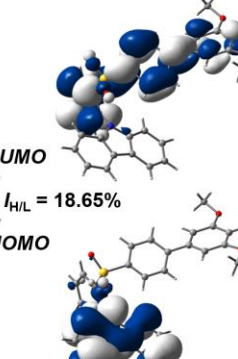
Compounds	Frontier Orbitals	Overlapped Orbitals
2CzP	 <p style="text-align: center;"><i>HOMO</i> $I_{H/L} = 15.79\%$ <i>LUMO</i></p>	<i>Not found</i>
2CzOC	 <p style="text-align: center;"><i>HOMO</i> $I_{H/L} = 16.50\%$ <i>LUMO</i></p>	 <i>LUMO+3</i>
2CzOC2	 <p style="text-align: center;"><i>HOMO</i> $I_{H/L} = 18.16\%$ <i>LUMO</i></p>	<i>Not found</i>
2CzOC3	 <p style="text-align: center;"><i>HOMO</i> $I_{H/L} = 18.65\%$ <i>LUMO</i></p>	<i>Not found</i>

Figure S24. Frontier orbitals and the overlapped orbitals in *ortho*-substituents (isovalue = 0.02).

SUPPORTING INFORMATION

Table S2. Spin-orbit coupling (SOC) constants between the lowest singlet and low-lying triplet states.

SOC/cm ⁻¹	4CzP	4CzOC	4CzOC2	4CzOC3	2CzP	2CzOC	2CzOC2	2CzOC3
$\xi(S_1-T_1)$	0.31	0.30	0.04	0.46	0.31	0.42	0.44	0.40
$\xi(S_1-T_2)$	0.86	0.96	0.53	0.79	0.24	0.13	0.21	0.14
$\xi(S_1-T_3)$	0.38	0.34	0.13	0.26	0.09	-	-	0.27
$\xi(S_1-T_4)$	0.21	0.43	1.62	0.18	-	-	-	-
$\xi(S_1-T_5)$	-	-	0.38	-	-	-	-	-

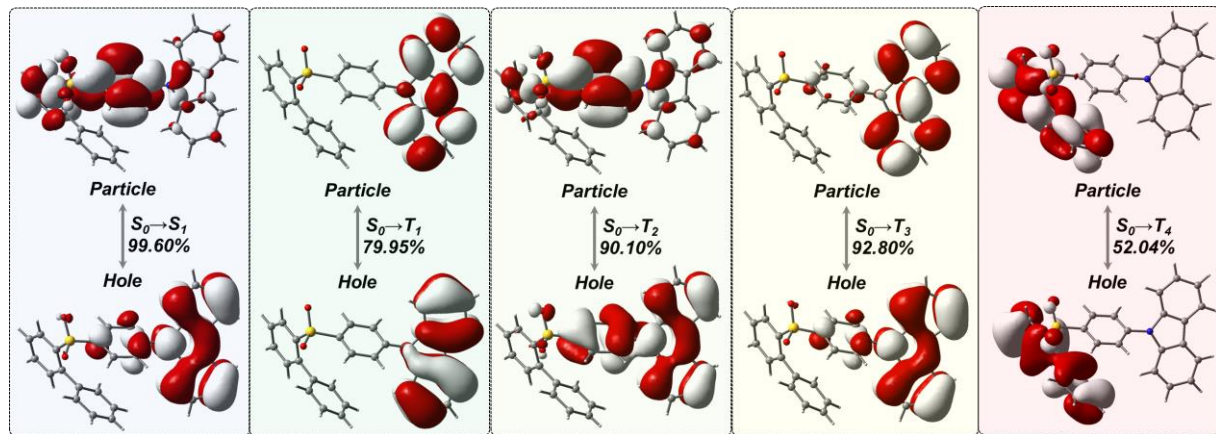


Figure S25. NTO analysis on $S_0 \rightarrow S_1$ and lower-lying $S_0 \rightarrow T_n$ states of 4CzP (isovalue = 0.02).

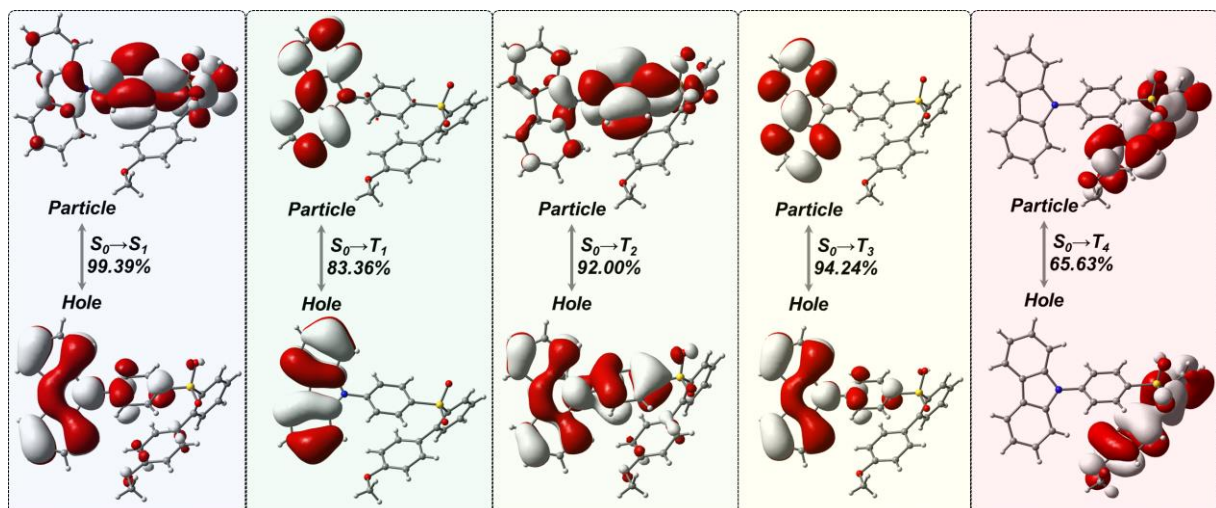


Figure S26. NTO analysis on $S_0 \rightarrow S_1$ and lower-lying $S_0 \rightarrow T_n$ states of 4CzOC (isovalue = 0.02).

SUPPORTING INFORMATION

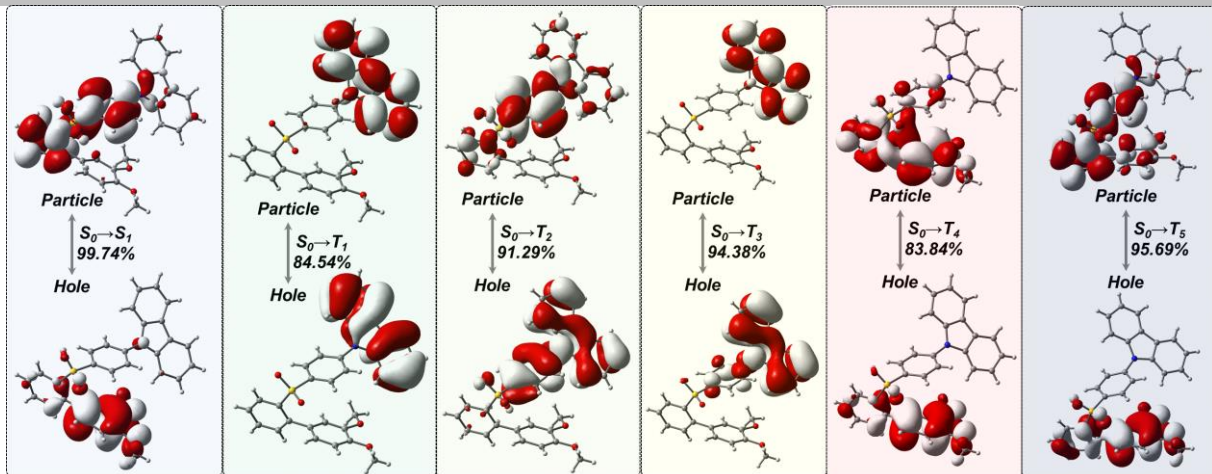


Figure S27. NTO analysis on $S_0 \rightarrow S_1$ and lower-lying $S_0 \rightarrow T_n$ states of 4CzOC2 (isovalue = 0.02).

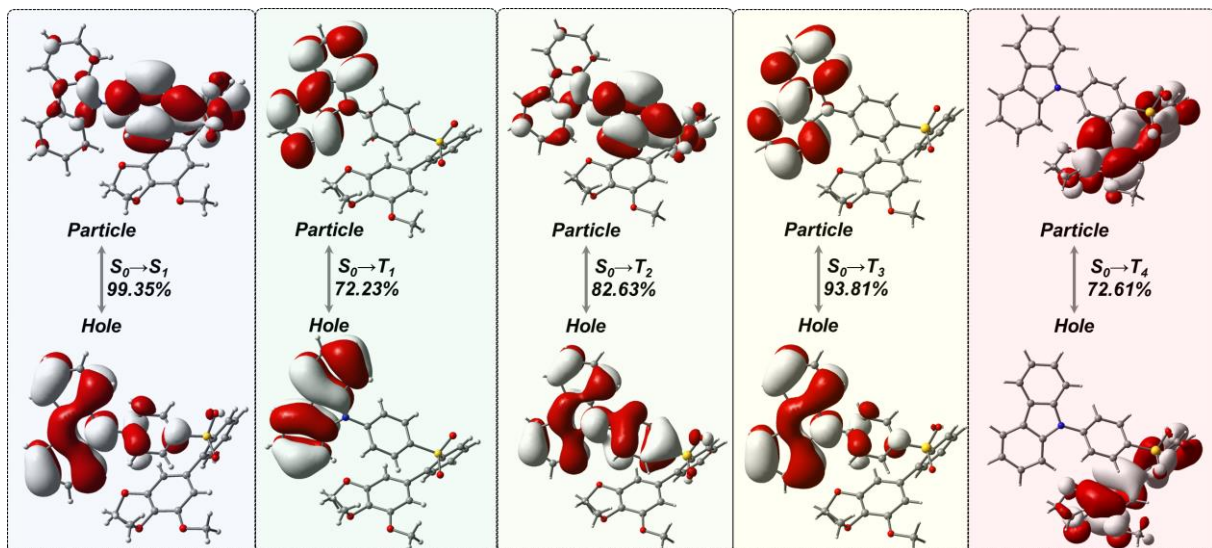


Figure S28. NTO analysis on $S_0 \rightarrow S_1$ and lower-lying $S_0 \rightarrow T_n$ states of 4CzOC3 (isovalue = 0.02).

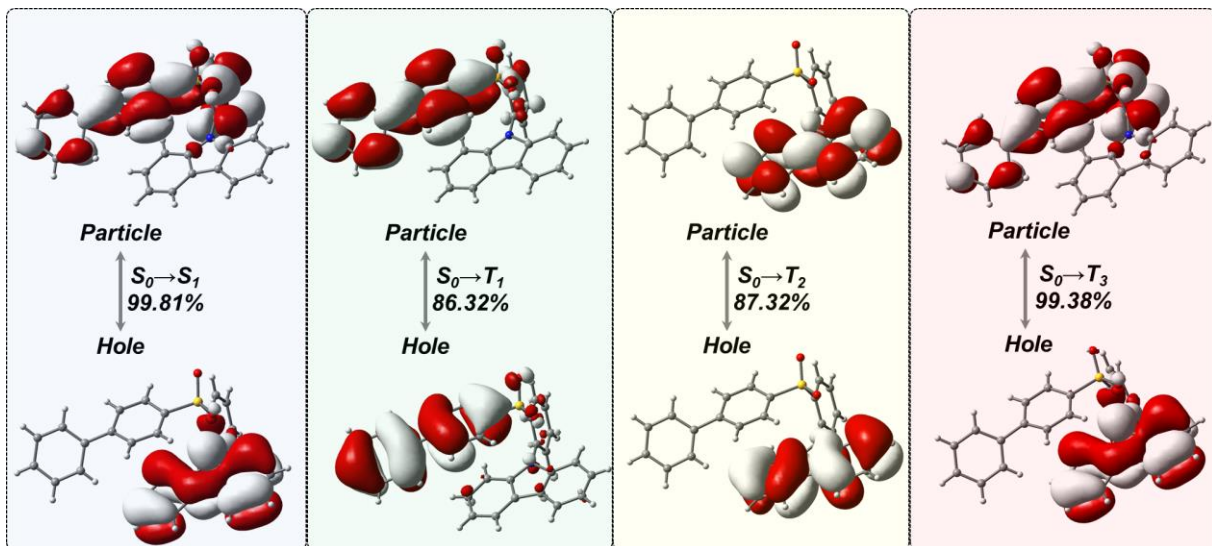


Figure S29. NTO analysis on $S_0 \rightarrow S_1$ and lower-lying $S_0 \rightarrow T_n$ states of 2CzP (isovalue = 0.02).

SUPPORTING INFORMATION

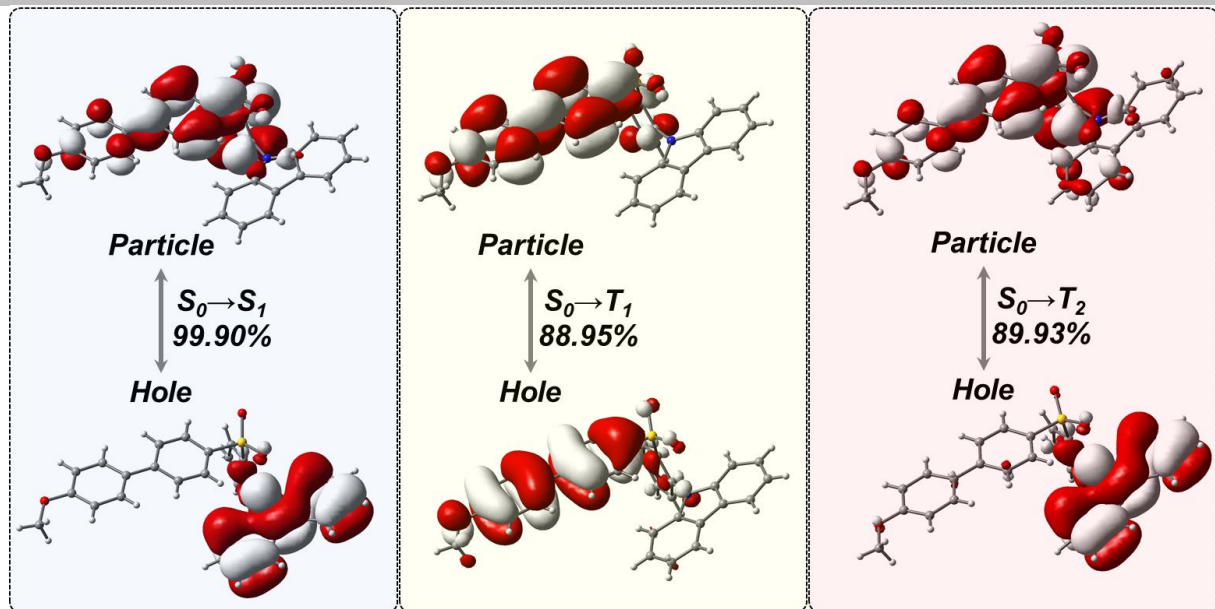


Figure S30. NTO analysis on $S_0 \rightarrow S_1$ and lower-lying $S_0 \rightarrow T_n$ states of 2CzOC (isovalue = 0.02).

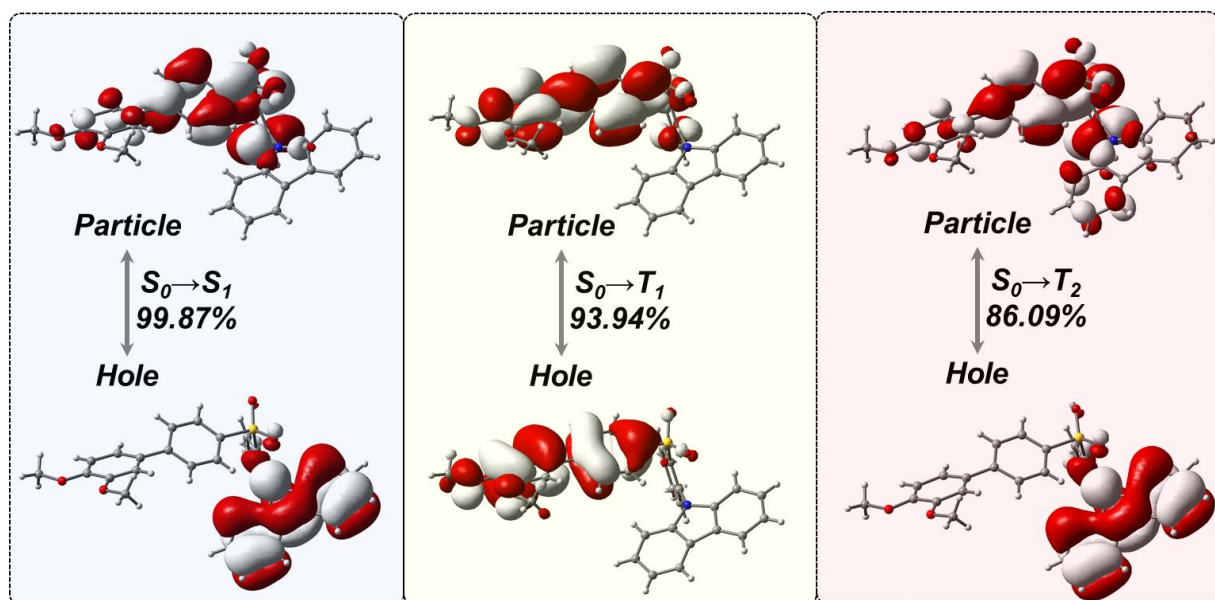


Figure S31. NTO analysis on $S_0 \rightarrow S_1$ and lower-lying $S_0 \rightarrow T_n$ states of 2CzOC2 (isovalue = 0.02).

SUPPORTING INFORMATION

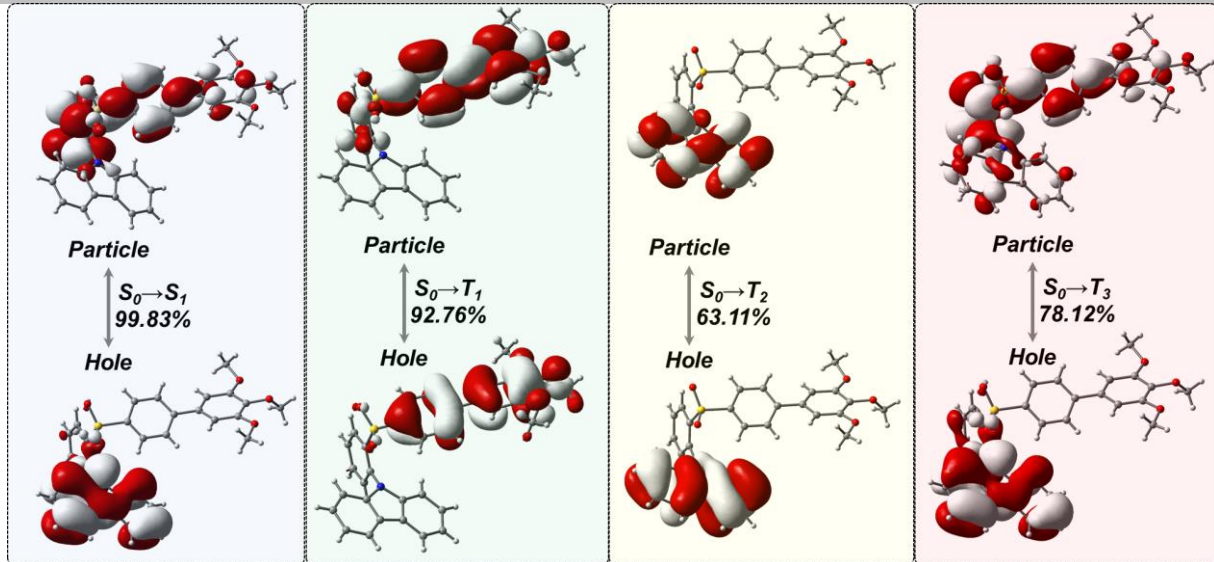


Figure S32. NTO analysis on $S_0 \rightarrow S_1$ and lower-lying $S_0 \rightarrow T_n$ states of 2CzOC3 (isovalue = 0.02).

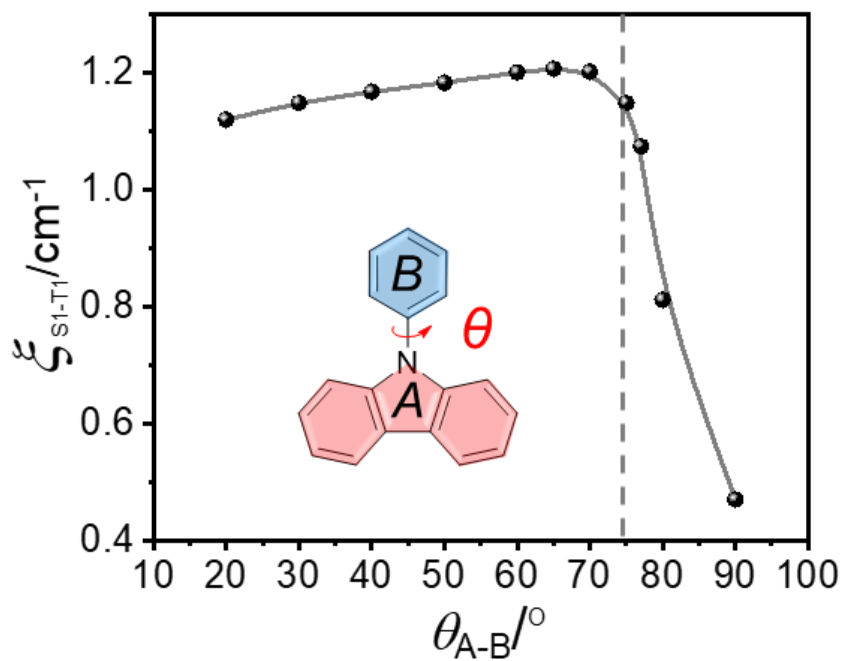


Figure S33. Dihedral angle depended spin-orbit coupling constants between S_1 and T_1 states of 9-phenyl-carbazole.

SUPPORTING INFORMATION

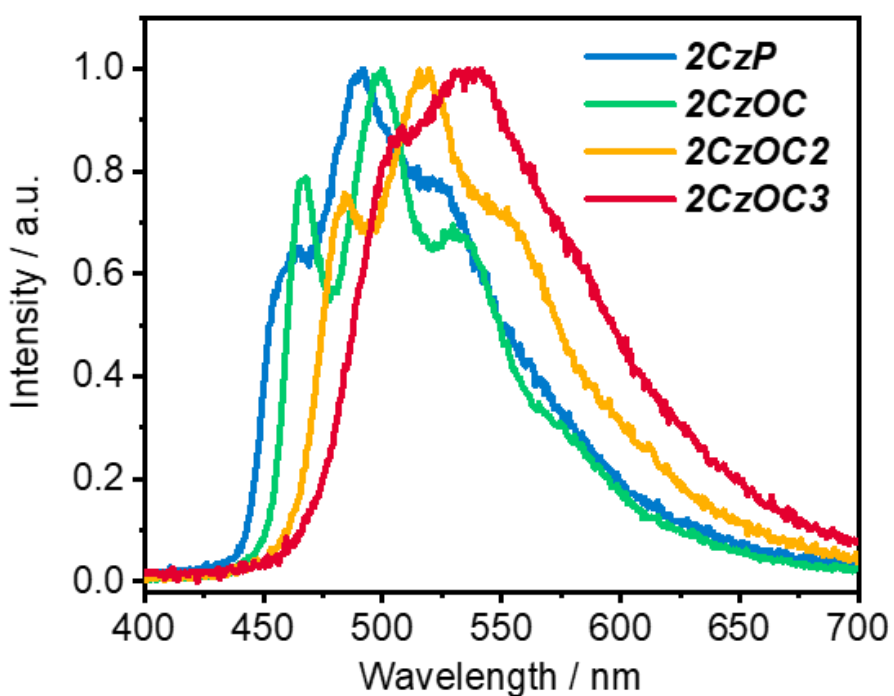


Figure S34. Phosphorescence spectra of *ortho*-substituents in dilute THF solutions at 77 K ($\sim 10^{-5}$ M, delayed time = 8 ms).

SUPPORTING INFORMATION

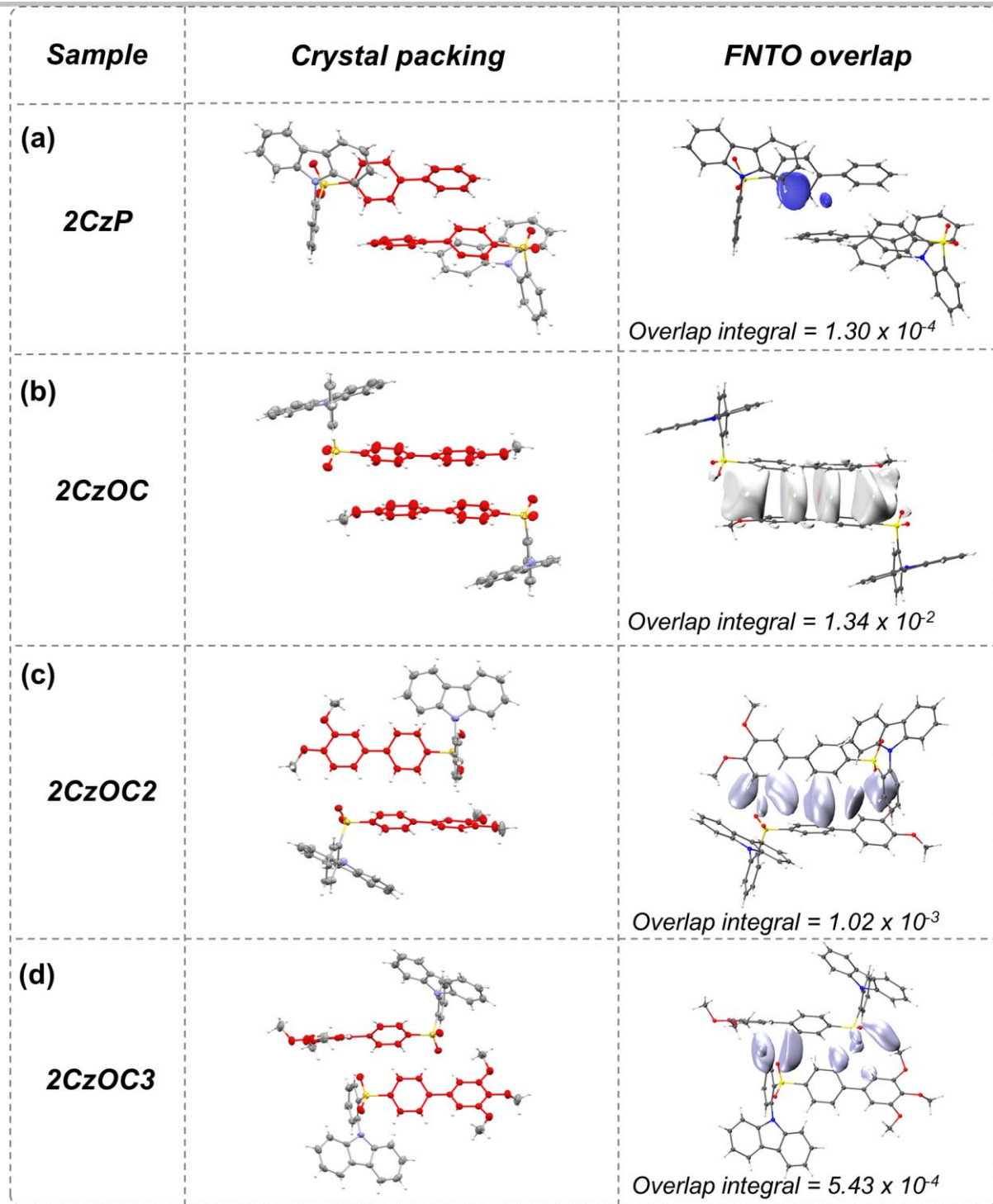


Figure S35. Packing modes in the single crystals and frontier natural transition orbital (FNTO, T₁ state) overlaps of (a) 2CzP; (b) 2CzOC; (c) 2CzOC2; (d) 2CzOC3. The red moieties contribute to the T₁ states (through NTO analysis) of these molecules. The FNTO (T₁) overlap between the adjacent molecules in space was visualized via isosurface volume with isovalue = 1×10^{-6} .

SUPPORTING INFORMATION

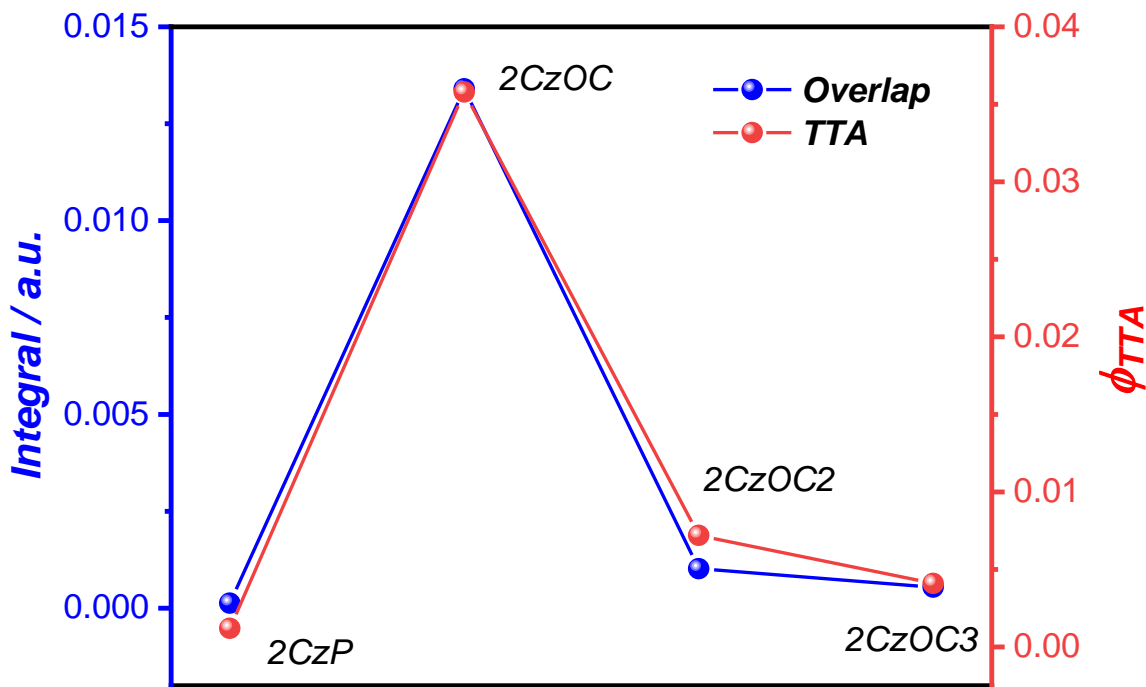


Figure S36. Correlation between the integral overlap of FNTO (T_1) and ϕ_{TTA} for *ortho*-substituents.

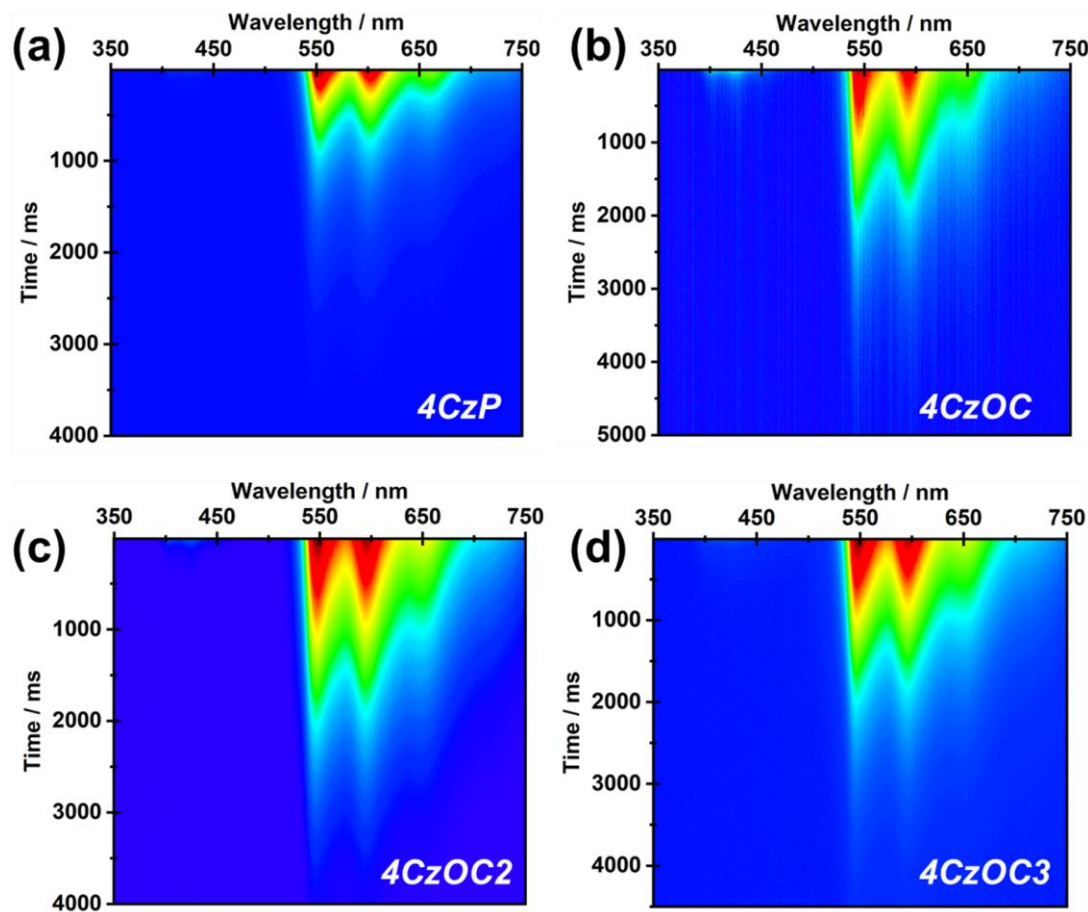


Figure S37. Time-resolved phosphorescence spectra of *para*-substituents under ambient conditions (excited with 365 nm, integral time = 8 ms).

SUPPORTING INFORMATION

2.3 Chemical characterization

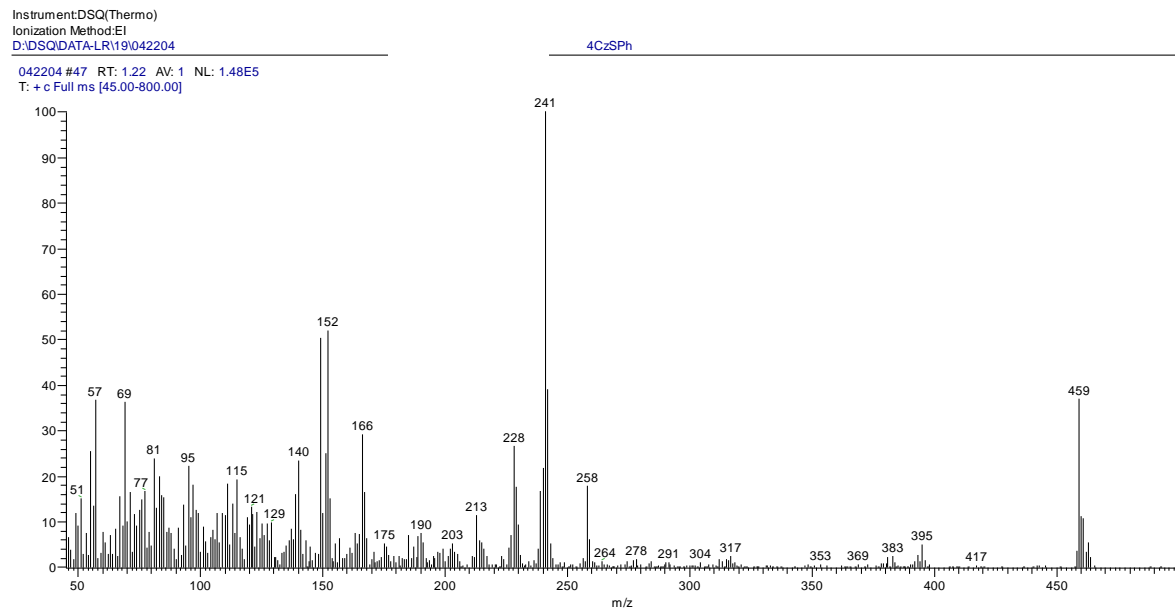


Figure S38. EI-MS of 4CzP.

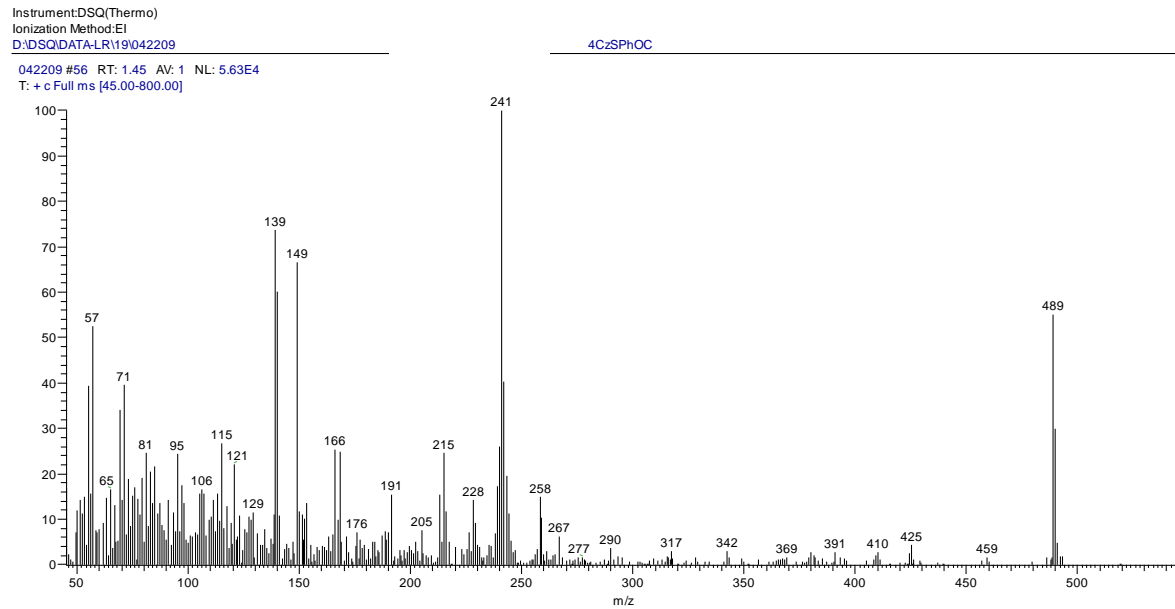


Figure S39. EI-MS of 4CzOC.

SUPPORTING INFORMATION

Instrument:DSQ(Thermo)
 Ionization Method:EI
 D:\DSQ\DATA-LR\19042210
 042210 #60 RT: 1.55 AV: 1 NL: 8.65E4
 T: + c Full ms [45.00-800.00]

4CzPh2OC

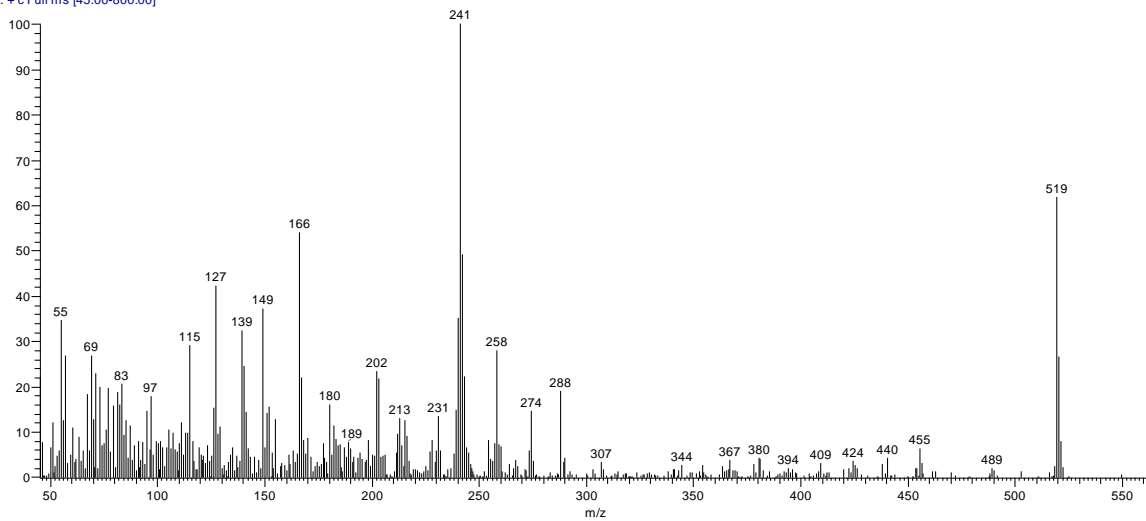


Figure S40. EI-MS of 4CzOC2.

Instrument:DSQ(Thermo)
 Ionization Method:EI
 D:\DSQ\DATA-LR\19042211
 042211 #72 RT: 1.86 AV: 1 NL: 4.52E5
 T: + c Full ms [45.00-800.00]

4CzPh3OC

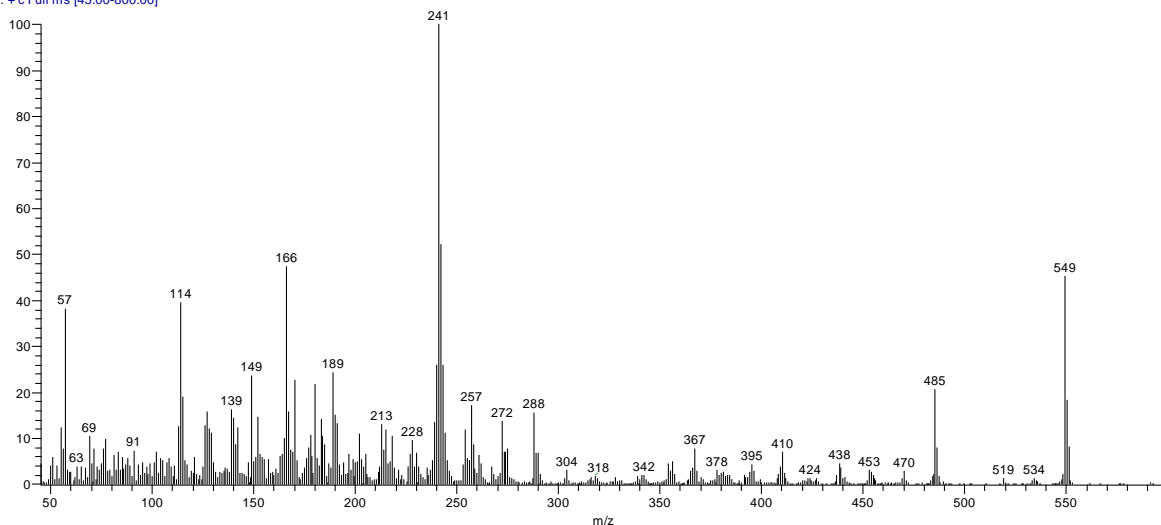


Figure S41. EI-MS of 4CzOC3.

SUPPORTING INFORMATION

Instrument:DSQ(Thermo)
 Ionization Method:EI
 D:\DSQ\DATA-LRV19\042201
 042201 #50 RT: 1.30 AV: 1 NL: 2.90E5
 T: + c Full ms [45.00-800.00]

2CzSPh

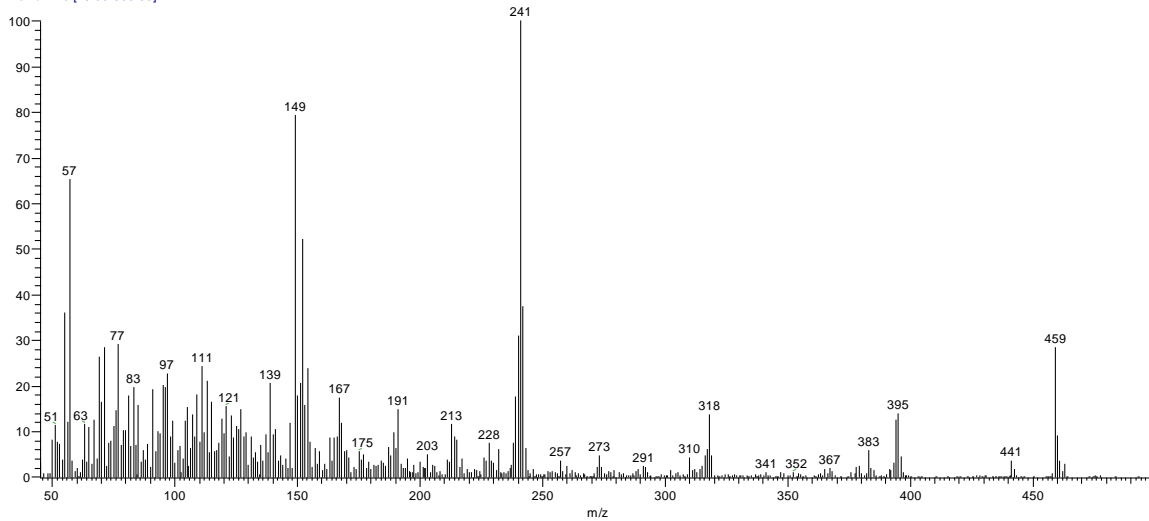


Figure S42. EI-MS of 2CzP.

Instrument:DSQ(Thermo)
 Ionization Method:EI
 D:\DSQ\DATA-LRV19\042205
 042205 #69 RT: 1.78 AV: 1 NL: 3.29E5
 T: + c Full ms [45.00-800.00]

2CzSPhOC

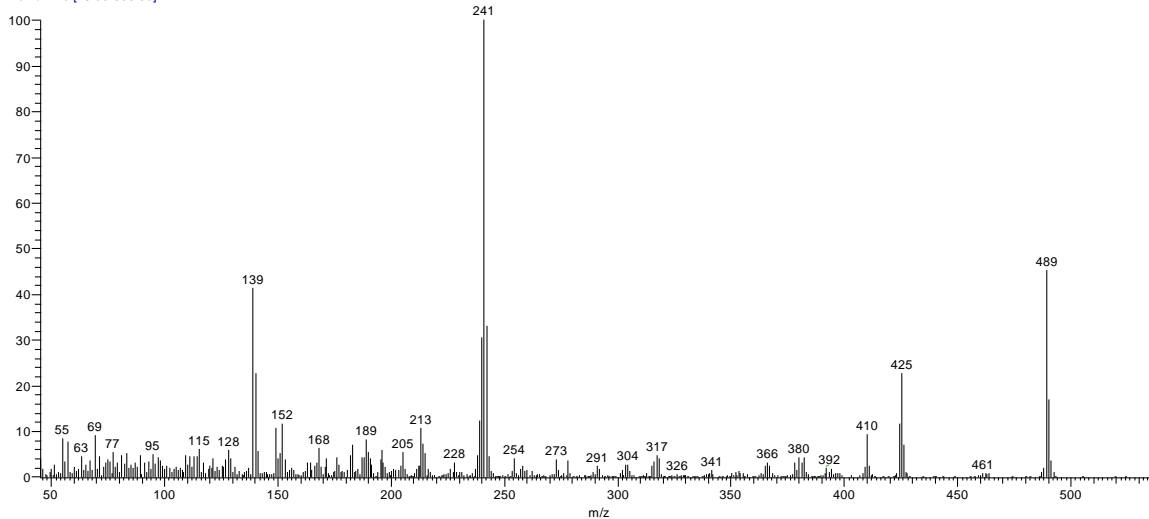


Figure S43. EI-MS of 2CzOC.

SUPPORTING INFORMATION

Instrument:DSQ(Thermo)
Ionization Method:EI
D:\DSQ\DATA-LR\19042206

042206 #67 RT: 1.73 AV: 1 NL: 1.77E5
T: + c Full ms [45.00-800.00]

2CzPh2OC

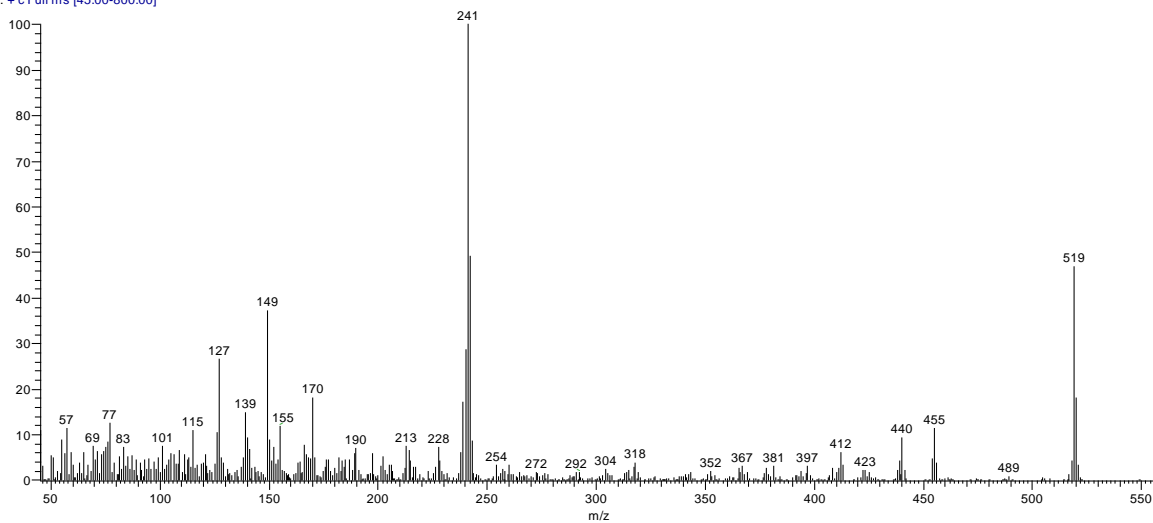


Figure S44. EI-MS of 2CzOC2.

Instrument:DSQ(Thermo)
Ionization Method:EI
D:\DSQ\DATA-LR\19042207

042207 #61 RT: 1.58 AV: 1 NL: 5.81E4
T: + c Full ms [45.00-800.00]

2CzPh3OC

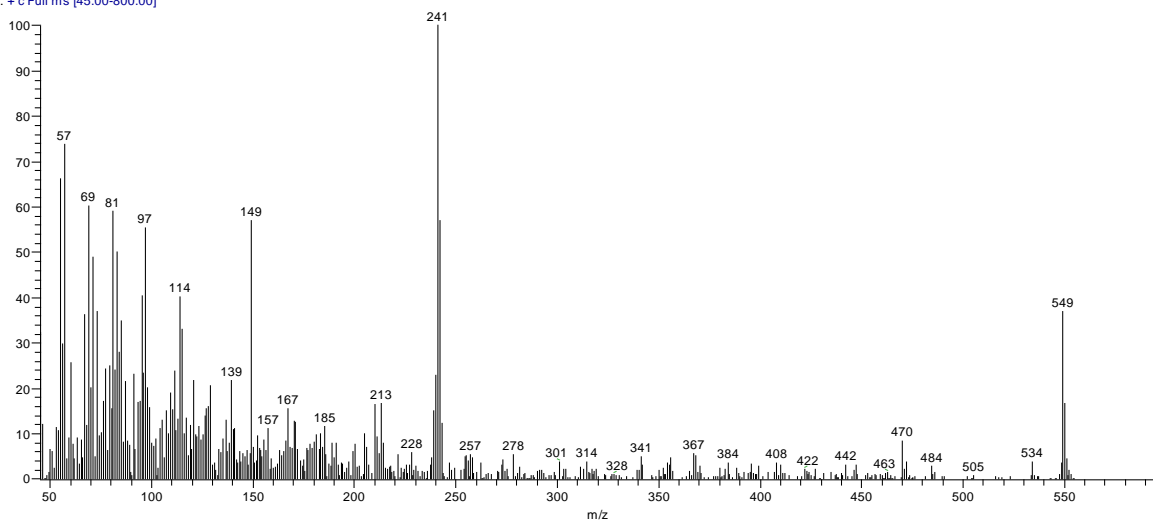


Figure S45. EI-MS of 2CzOC3.

SUPPORTING INFORMATION

Instrument: MAT 95XP(Thermo)
D:\DATA-HR\19042408-4czsph-c1
042408-4czsph-c1 #9 RT: 0.37 AV: 1 NL: 2.78E4
T: + c El Full ms [452.50-469.50]

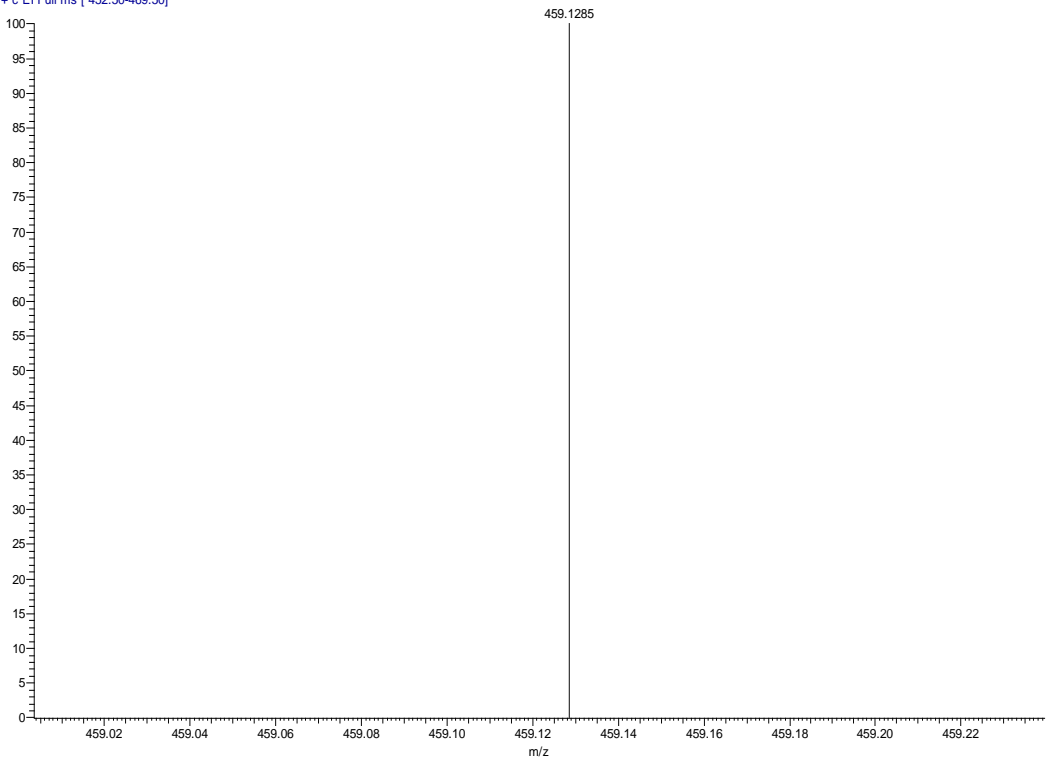


Figure S46. HRMS spectrum of 4CzP.

Instrument: MAT 95XP(Thermo)
D:\DATA-HR\19042406-4czsphoc-c1
042406-4czsphoc-c1 #5 RT: 0.22 AV: 1 NL: 2.01E4
T: + c El Full ms [478.50-495.50]

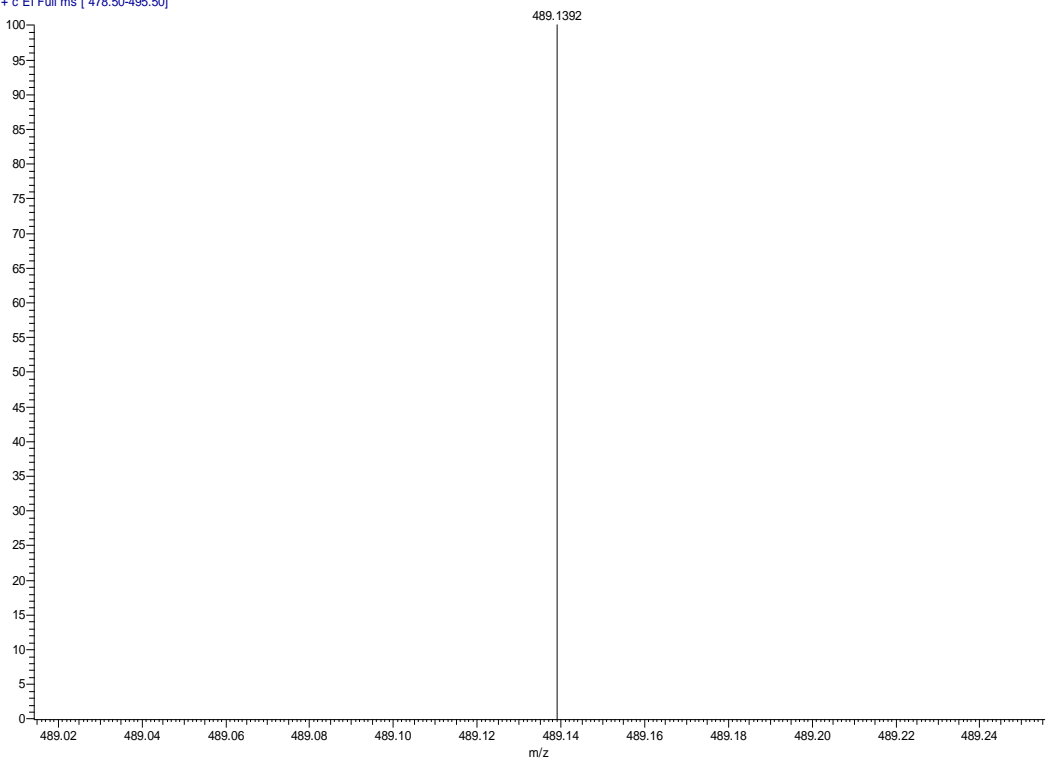


Figure S47. HRMS spectrum of 4CzOC.

SUPPORTING INFORMATION

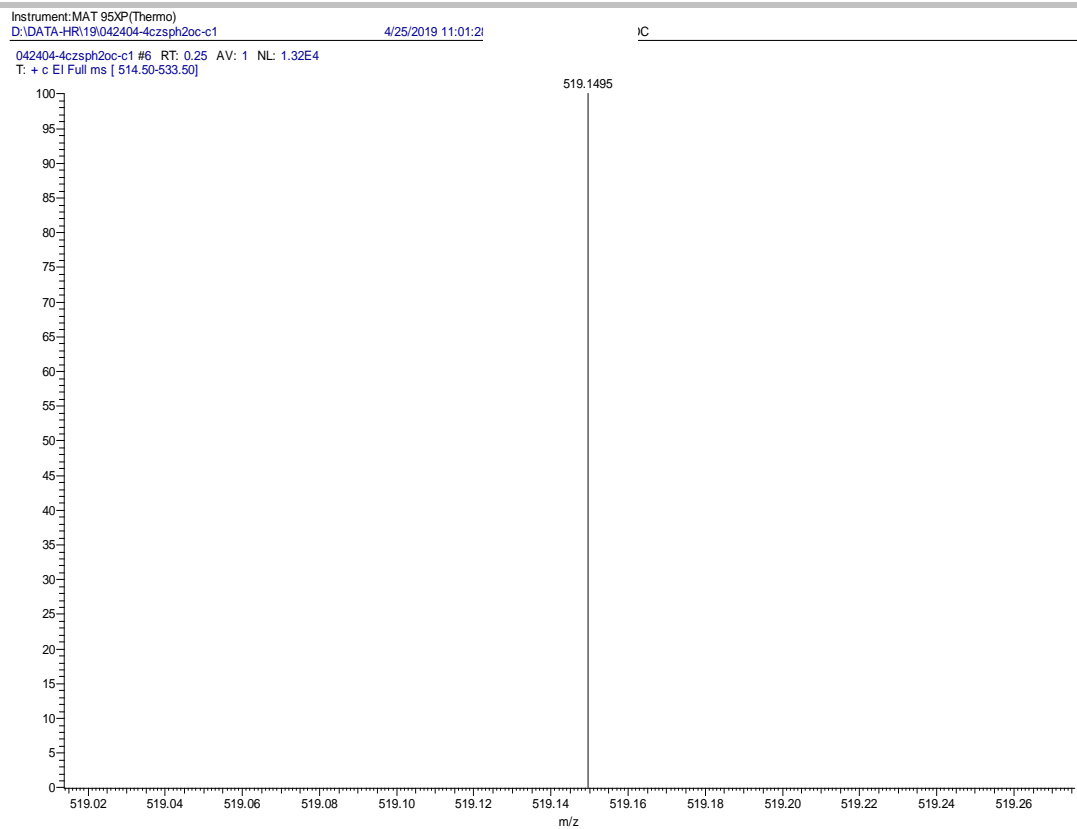


Figure S48. HRMS spectrum of 4CzOC2.

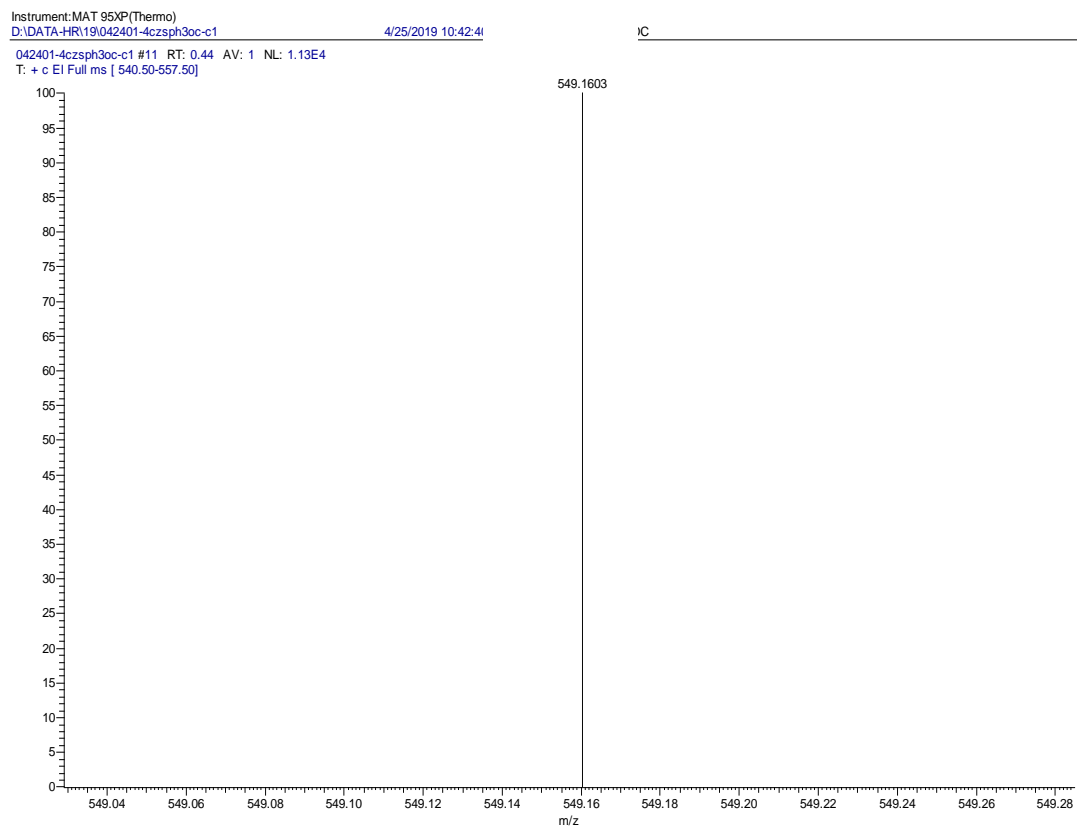


Figure S49. HRMS spectrum of 4CzOC3.

SUPPORTING INFORMATION

Instrument: MAT 95XP(Thermo)
D:\DATA-HR\19042407-2czsph-c1
042407-2czsph-c1 #5 RT: 0.19 AV: 1 NL: 1.38E4
T: + c EI Full ms [452.50-469.50]

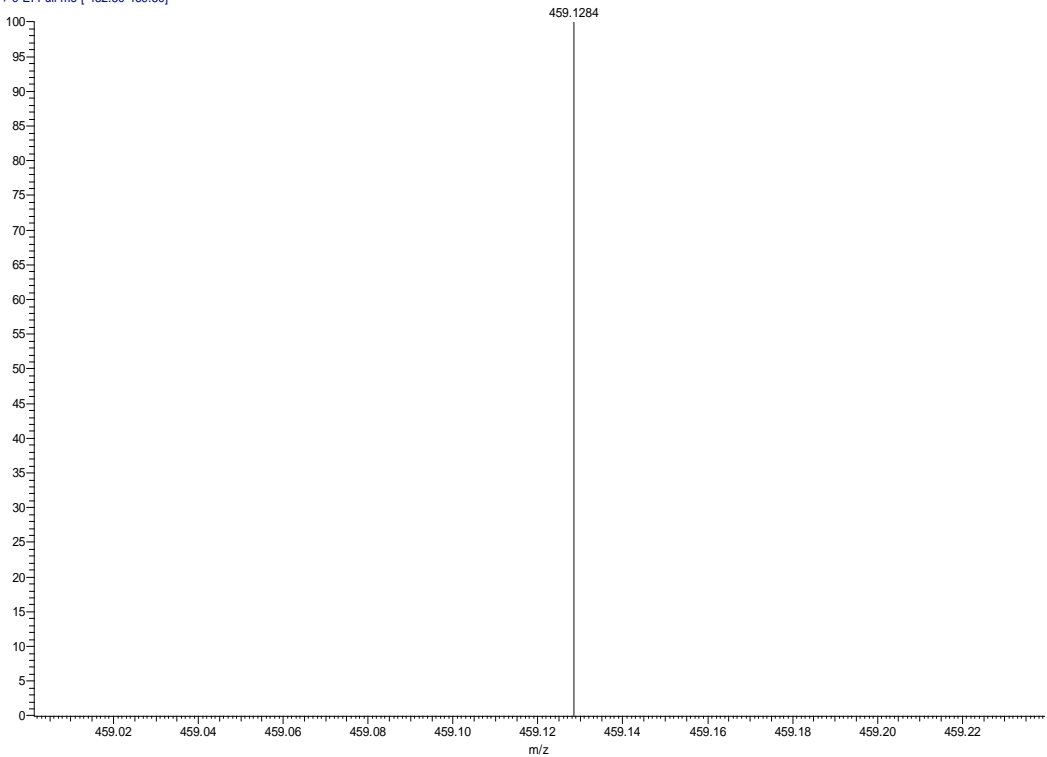


Figure S50. HRMS spectrum of 2CzP.

Instrument: MAT 95XP(Thermo)
D:\DATA-HR\19042405-2czsphoc-c1
042405-2czsphoc-c1 #11 RT: 0.41 AV: 1 NL: 4.73E4
T: + c EI Full ms [478.50-495.50]

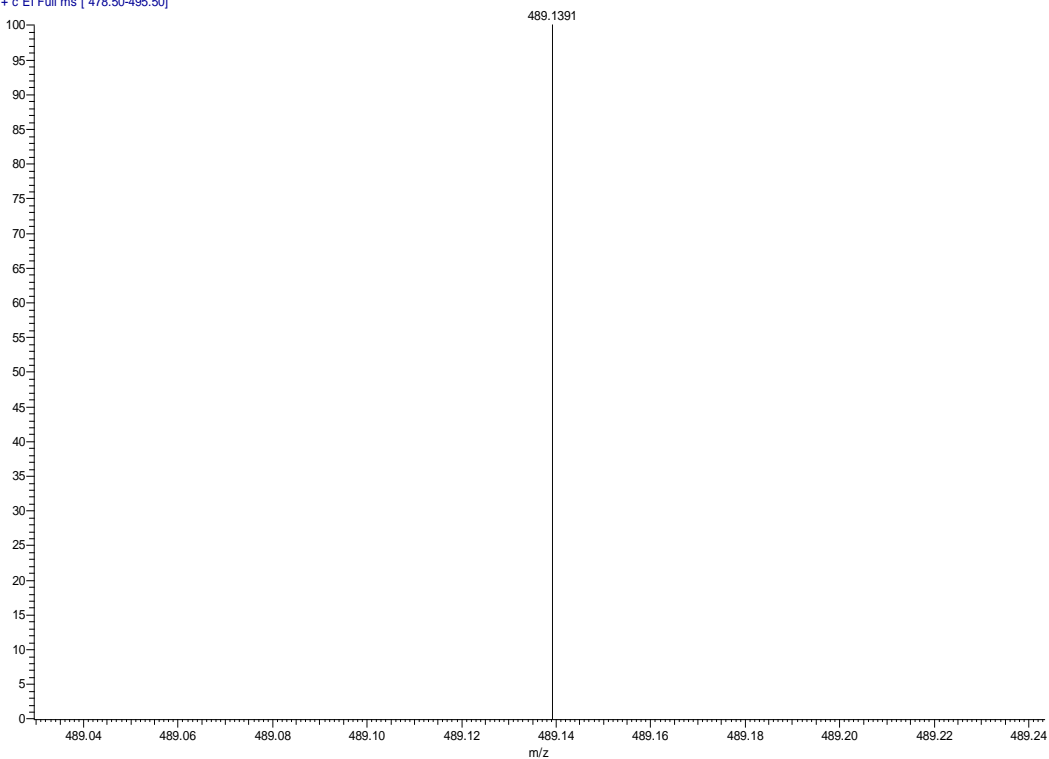


Figure S51. HRMS spectrum of 2CzOC.

SUPPORTING INFORMATION

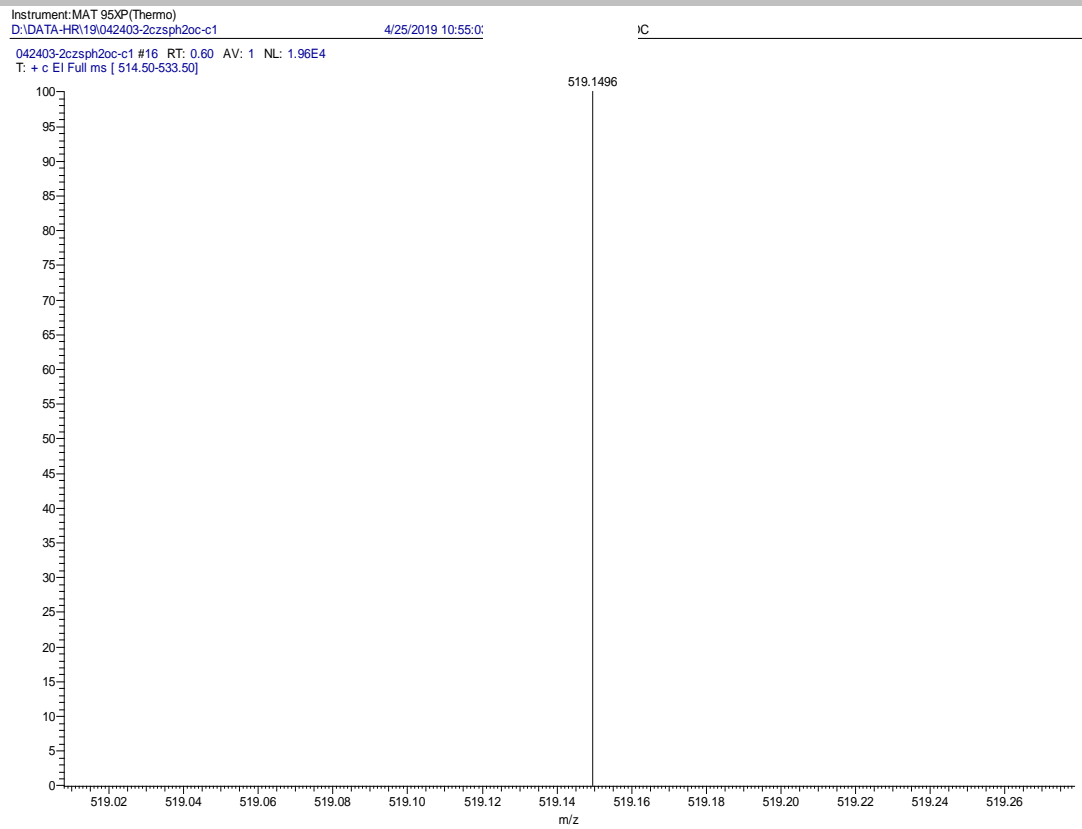


Figure S52. HRMS spectrum of 2CzOC2.

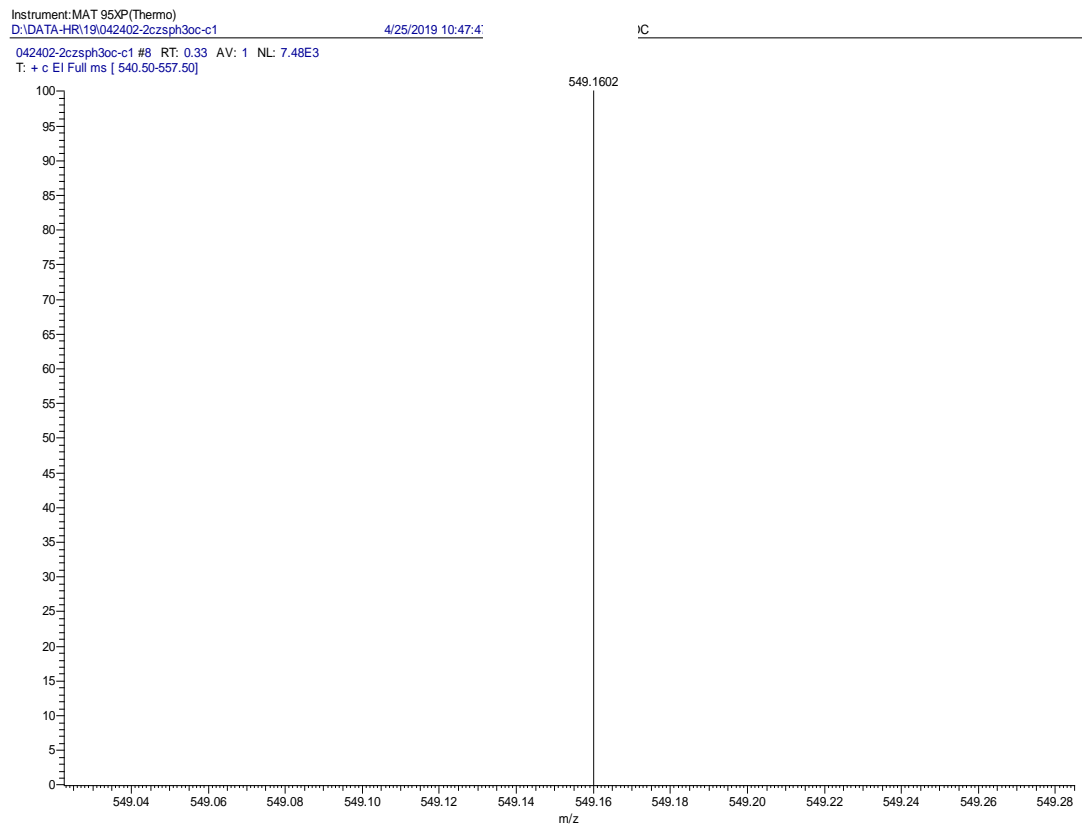


Figure S53. HRMS spectrum of 2CzOC3.

SUPPORTING INFORMATION

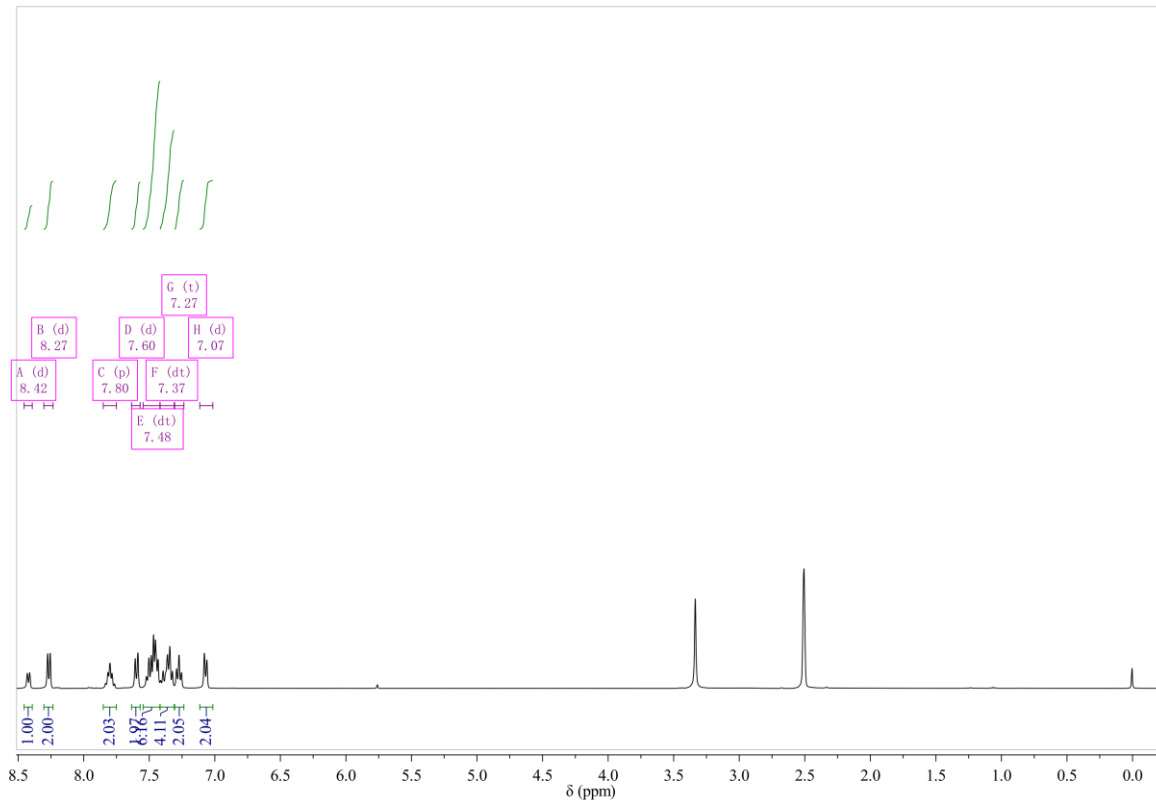


Figure S54. ¹H NMR spectrum of 4CzP.

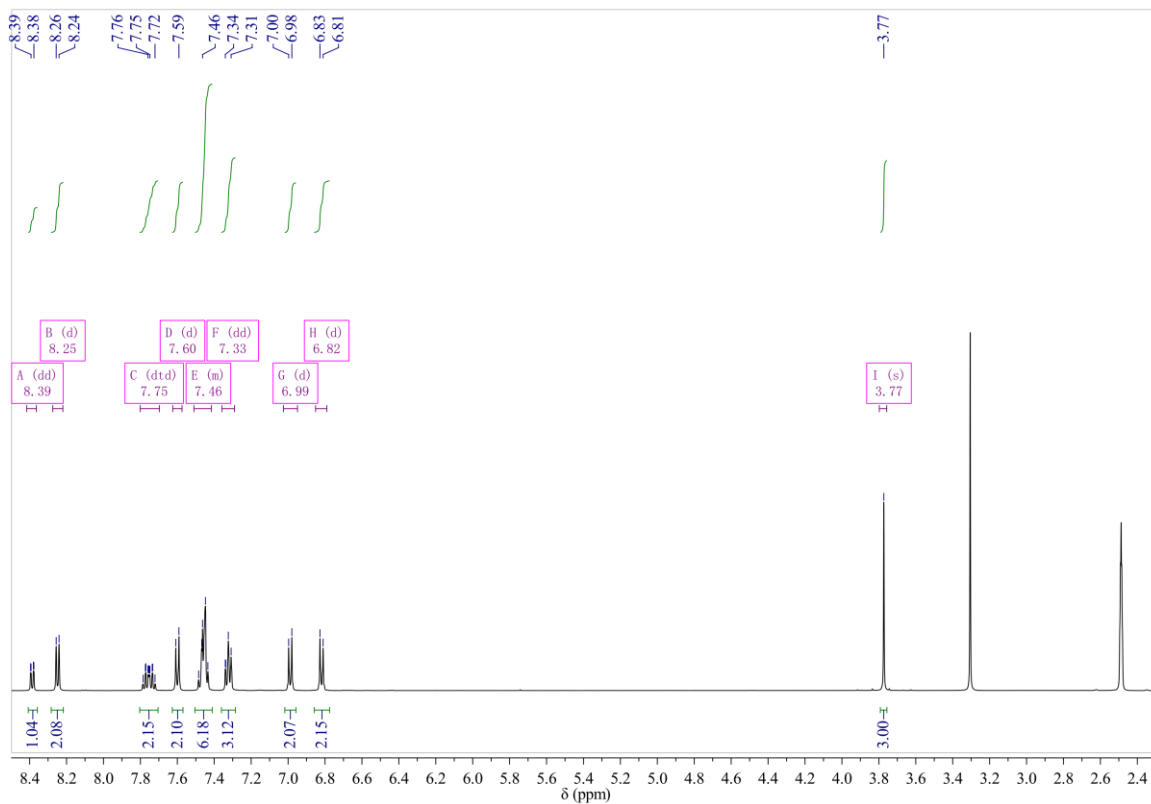


Figure S55. ¹H NMR spectrum of 4CzOC.

SUPPORTING INFORMATION

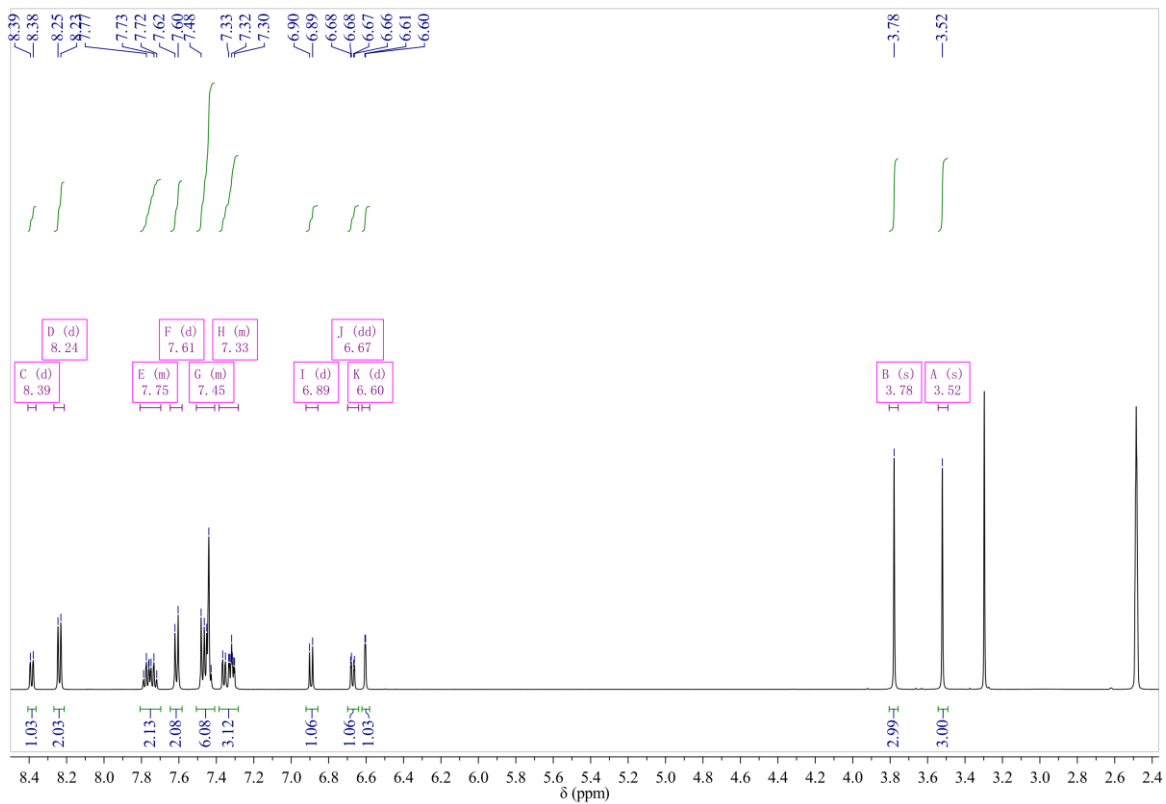


Figure S56. ^1H NMR spectrum of 4CzOC2.

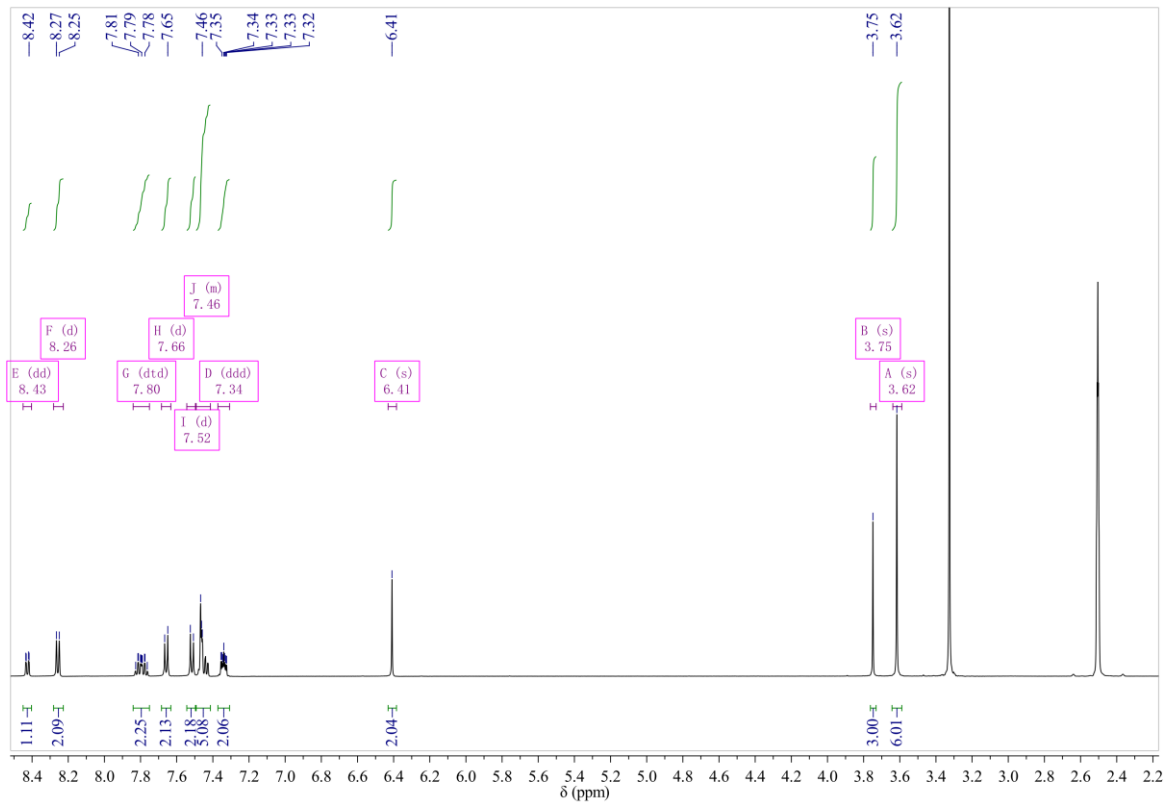


Figure S57. ^1H NMR spectrum of 4CzOC3.

SUPPORTING INFORMATION

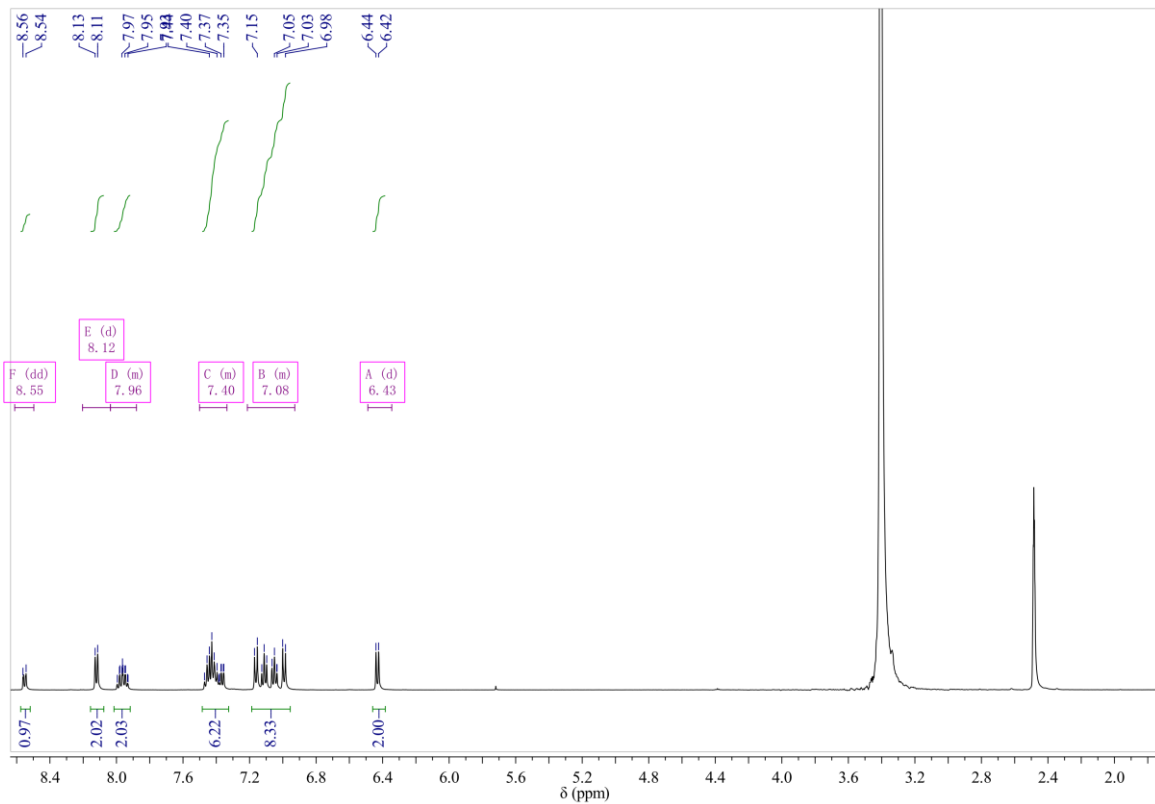


Figure S58. ¹H NMR spectrum of 2CzP.

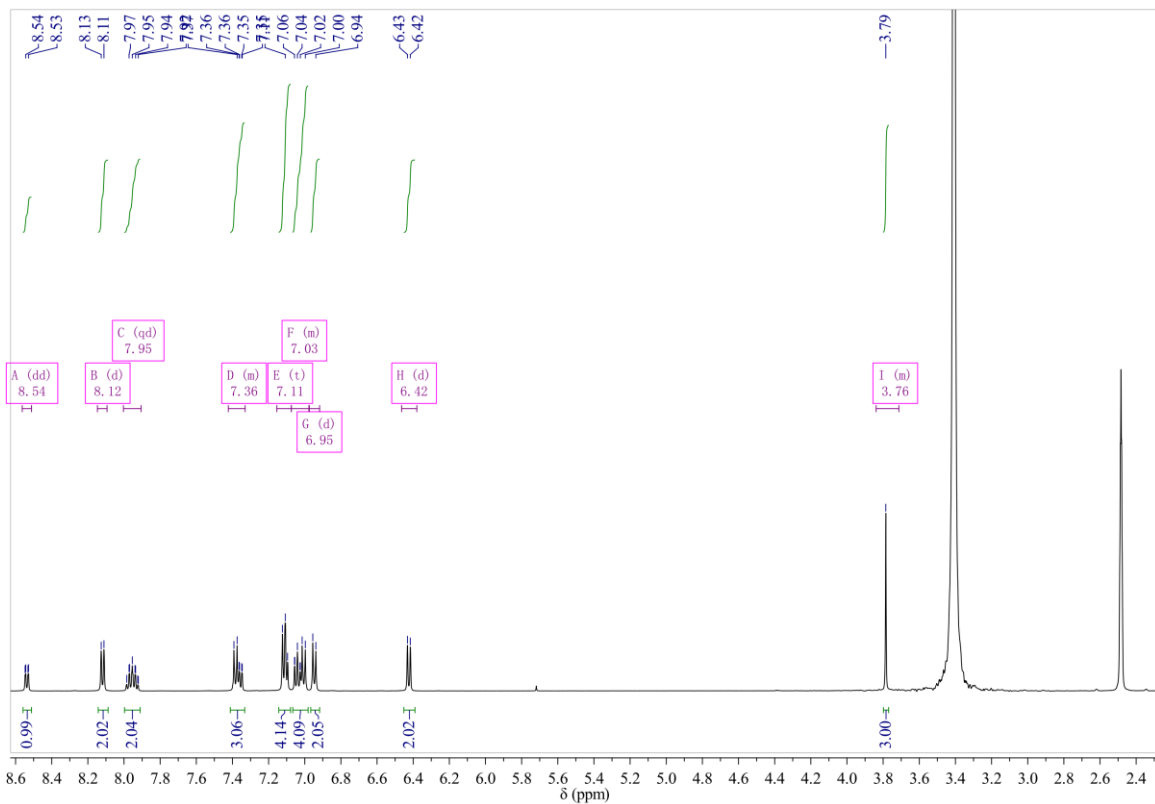


Figure S59. ¹H NMR spectrum of 2CzOC.

SUPPORTING INFORMATION

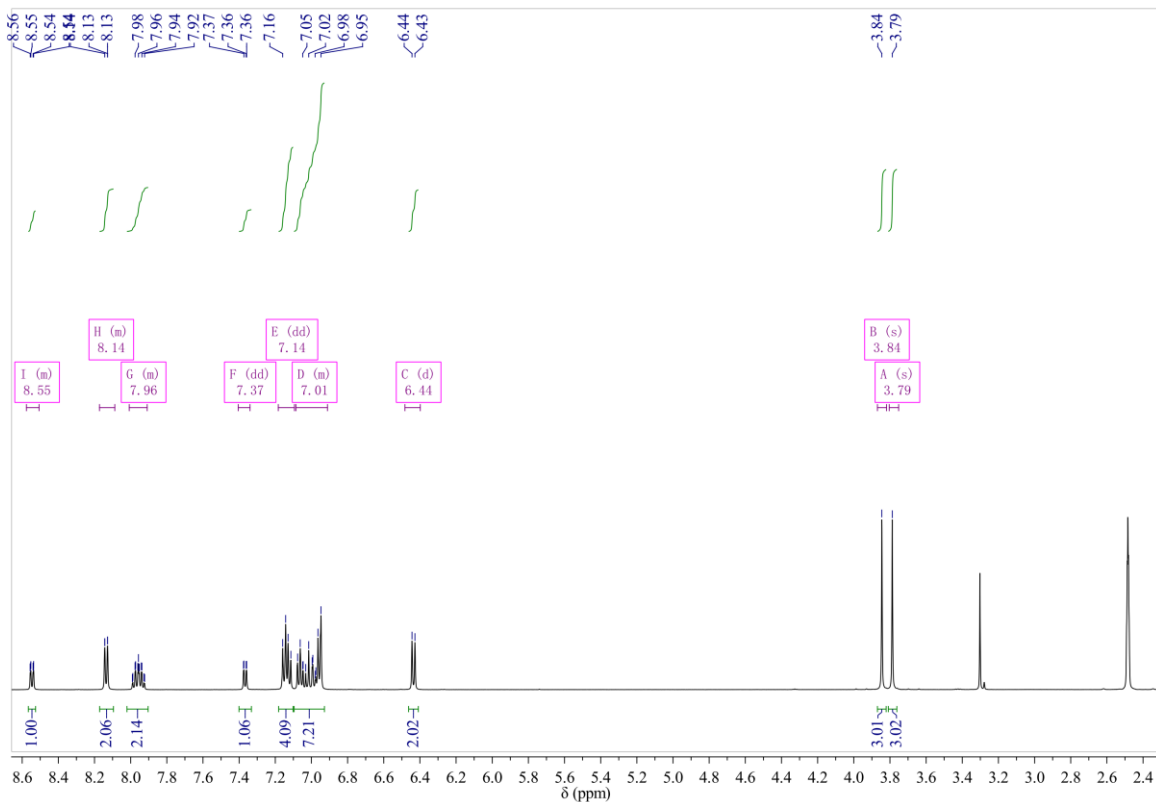


Figure S60. ¹H NMR spectrum of 2CzOC2.

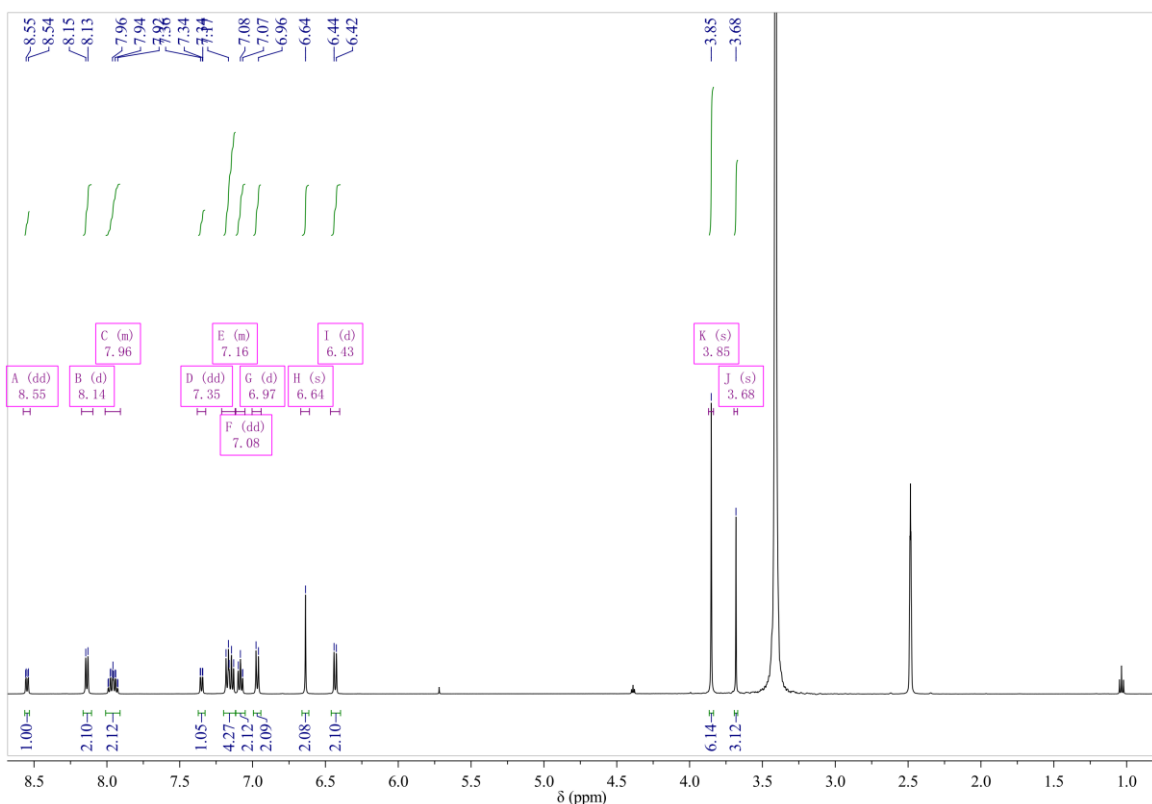


Figure S61. ¹H NMR spectrum of 2CzOC3.

SUPPORTING INFORMATION

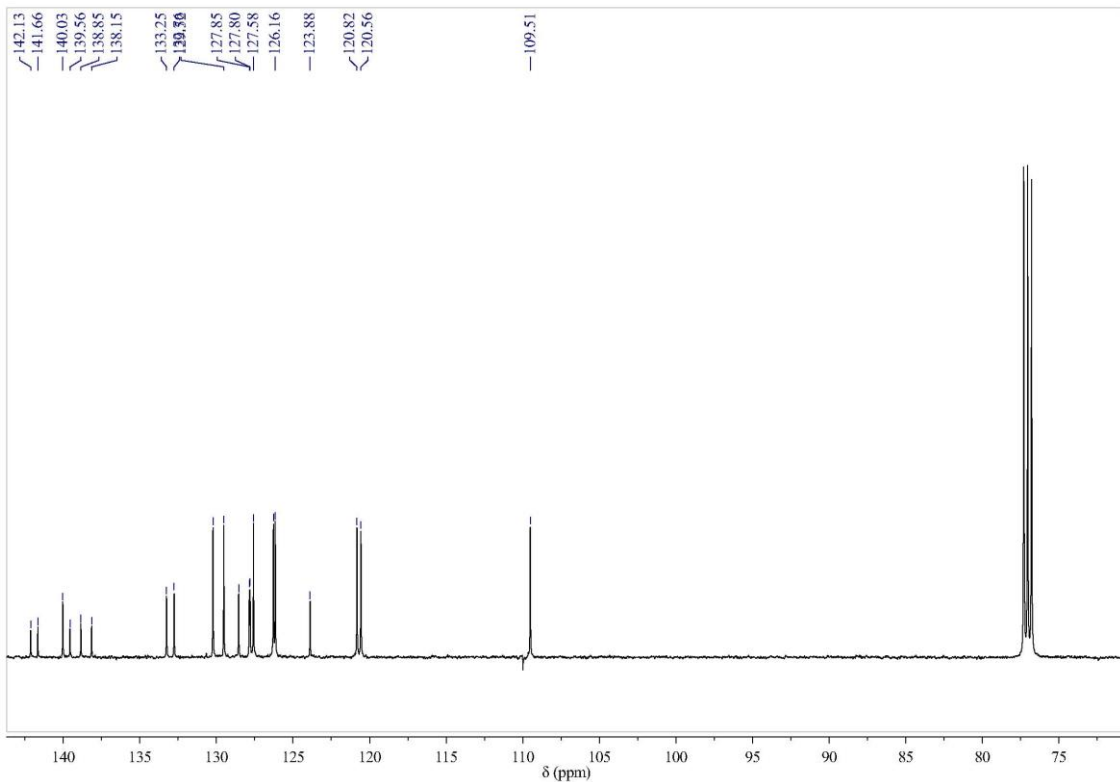


Figure S62. ¹³C NMR spectrum of 4CzP.

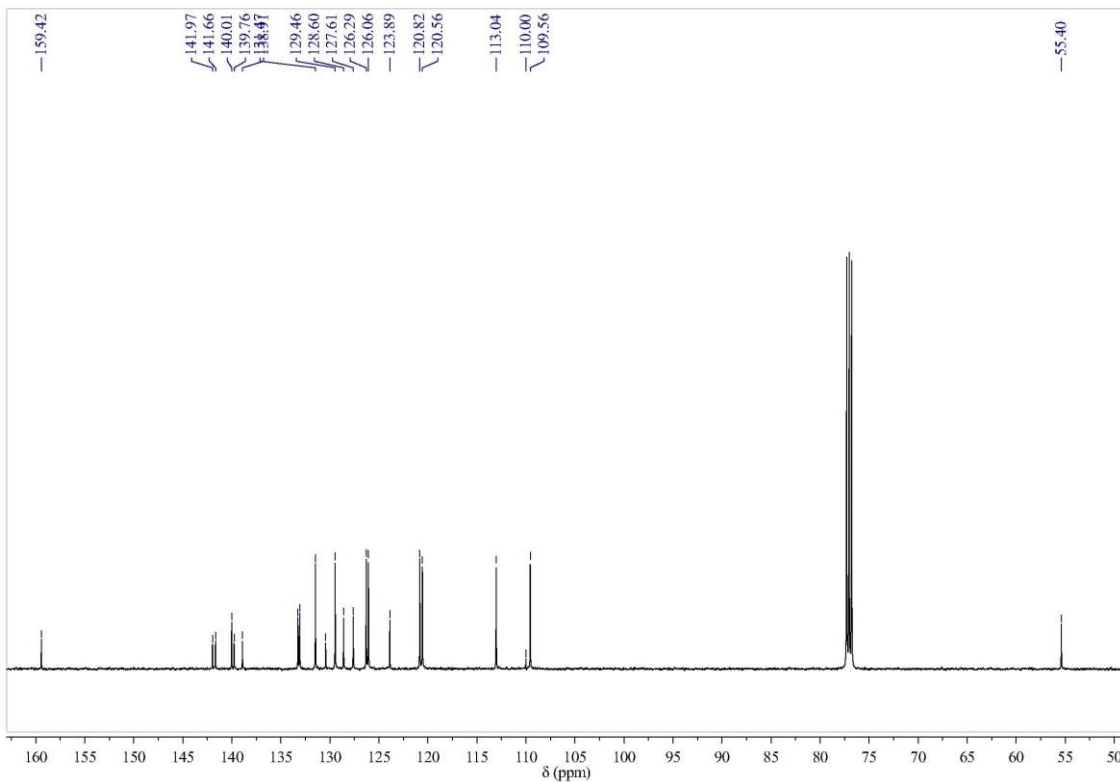


Figure S63. ¹³C NMR spectrum of 4CzOC.

SUPPORTING INFORMATION

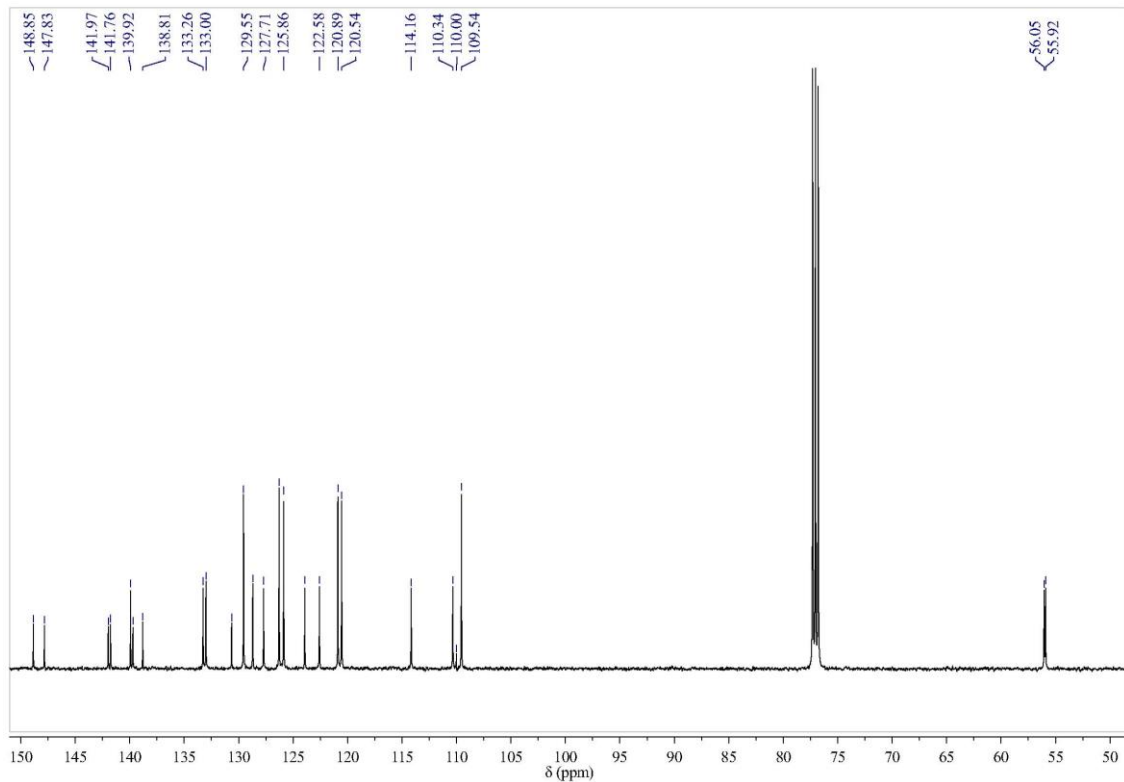


Figure S64. ^{13}C NMR spectrum of 4CzOC2.

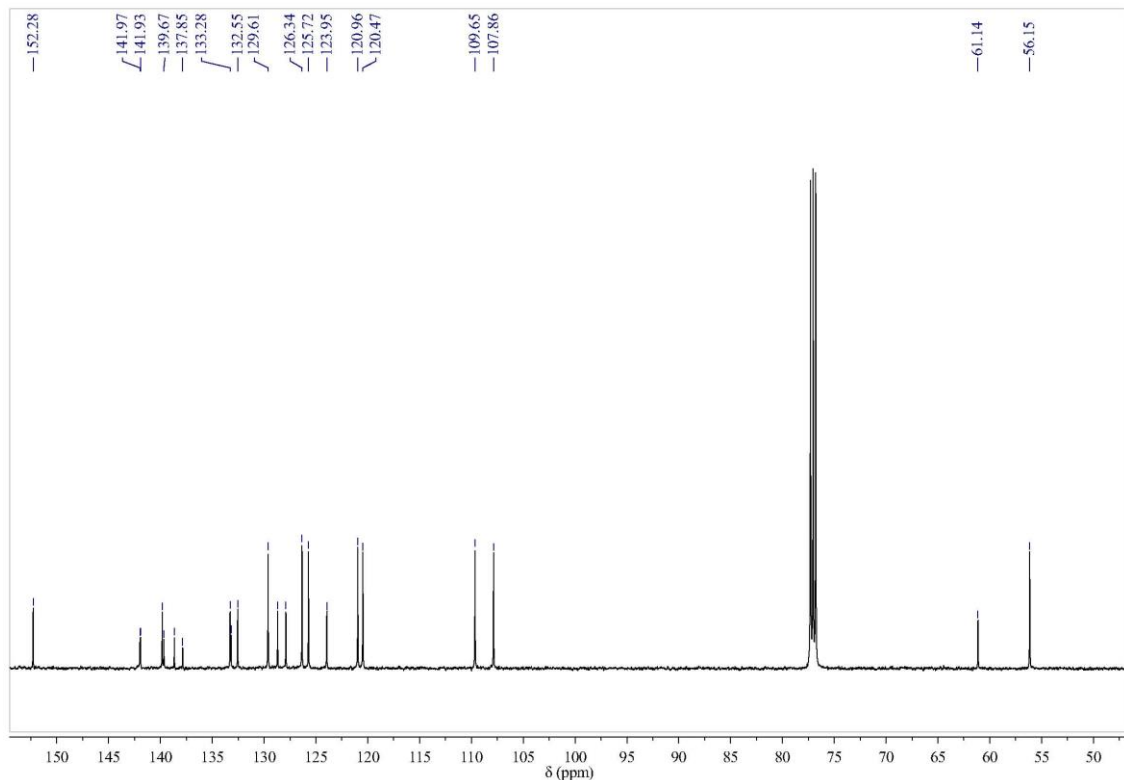


Figure S65. ^{13}C NMR spectrum of 4CzOC3.

SUPPORTING INFORMATION

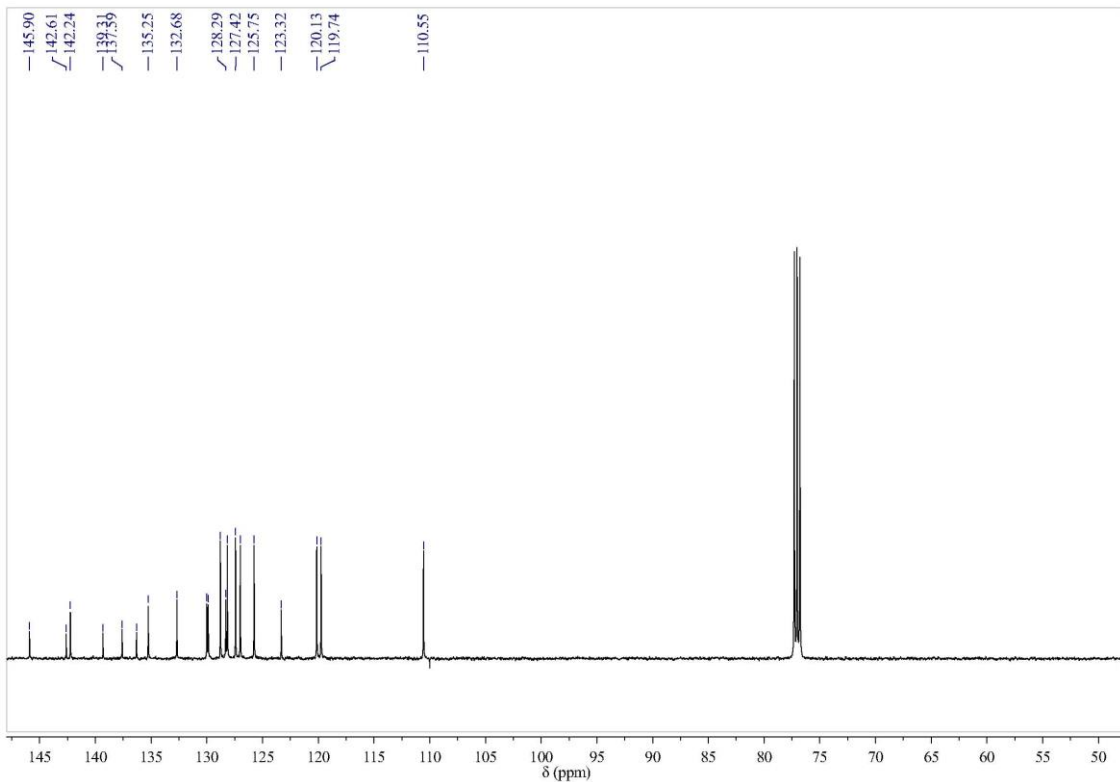


Figure S66. ¹³C NMR spectrum of 2CzP.

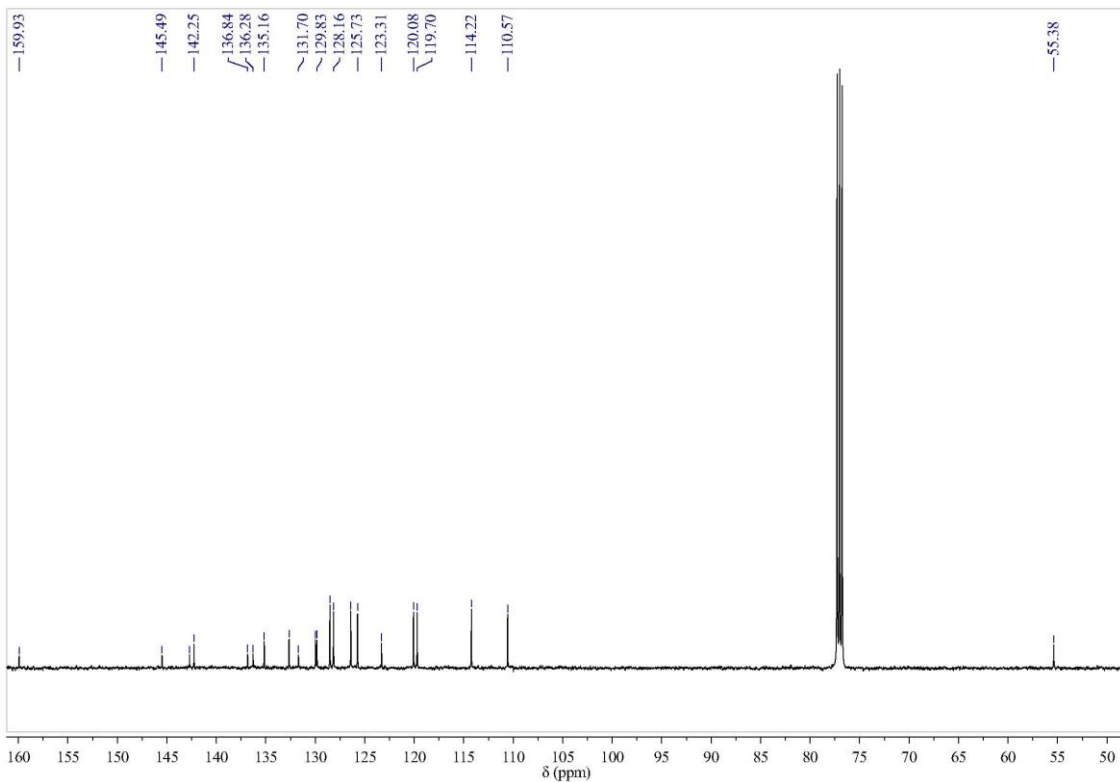


Figure S67. ¹³C NMR spectrum of 2CzOC.

SUPPORTING INFORMATION

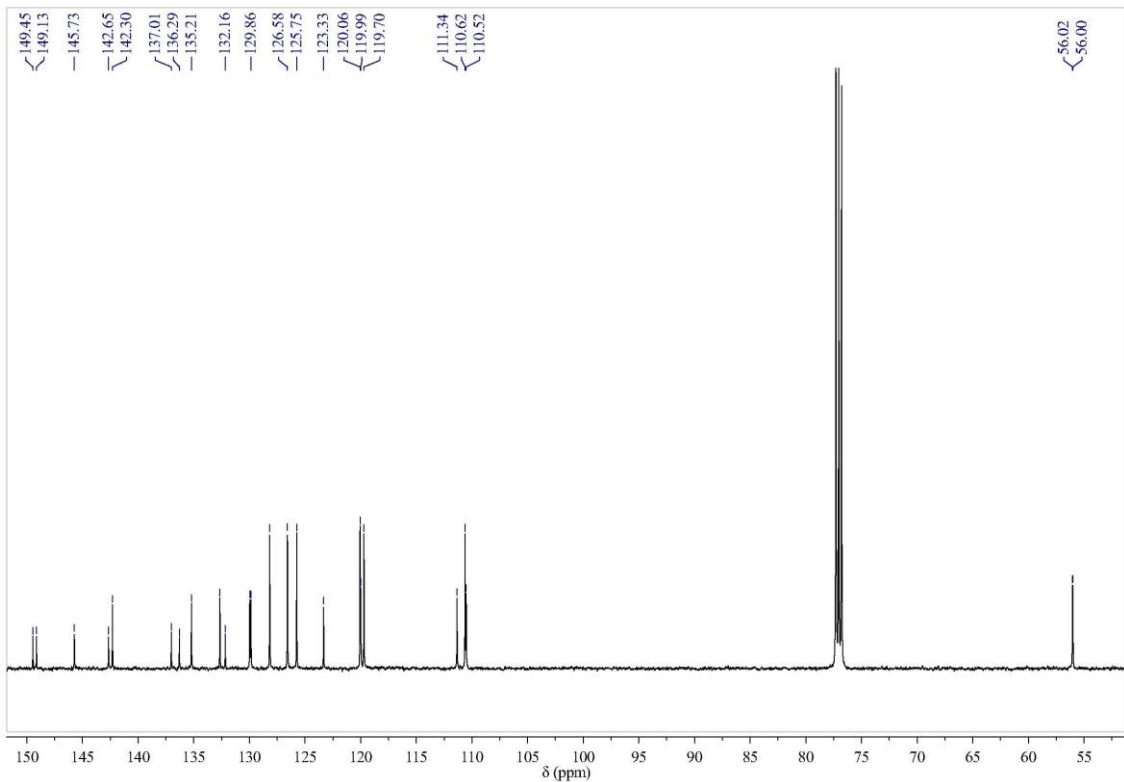


Figure S68. ¹³C NMR spectrum of 2CzOC2.

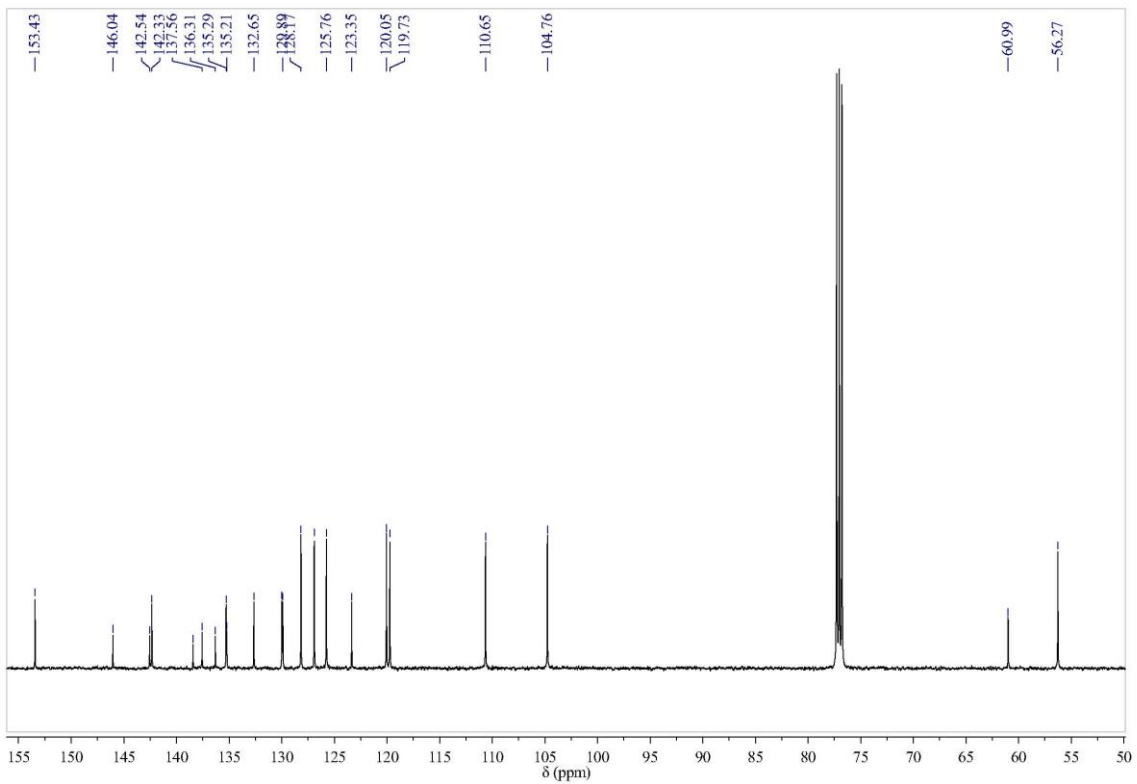


Figure S69. ¹³C NMR spectrum of 2CzOC3.

SUPPORTING INFORMATION

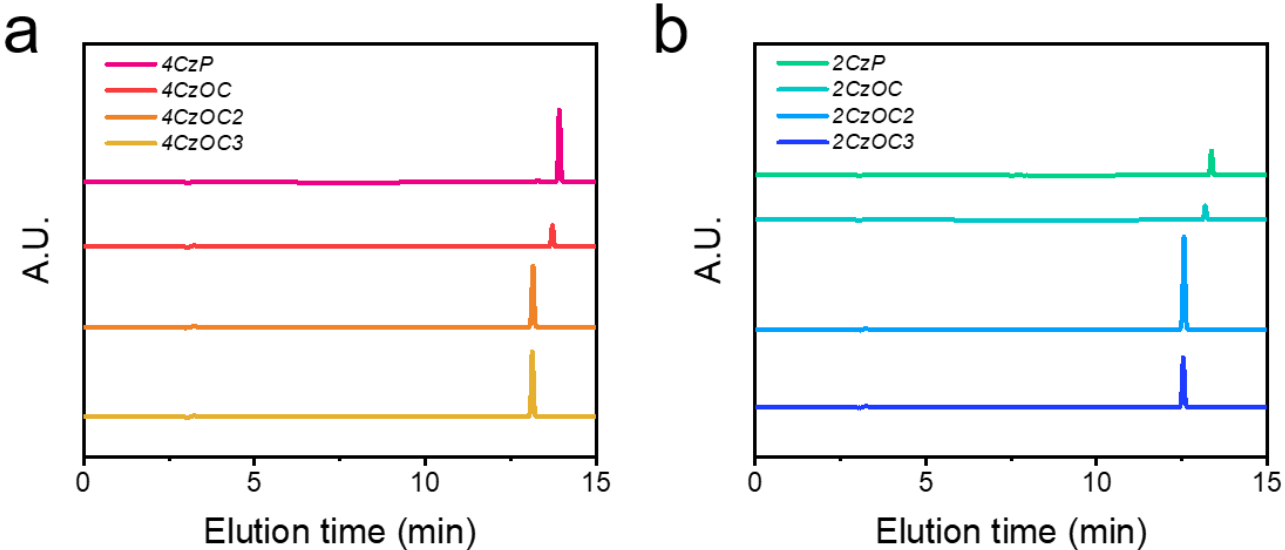


Figure S70. High-performance liquid chromatogram spectra of (a) 4CzP, 4CzOC, 4CzOC2 and 4CzOC3; (b) 2CzP, 2CzOC, 2CzOC2 and 4CzOC3 in acetonitrile solution. The peaks appearing around 3 min are the signals of solvent acetonitrile.

References

- [1] M. J. Frisch, G. W. Trucks, H. B. Schlegel, G. E. Scuseria, M. A. Robb, J. R. Cheeseman, G. Scalmani, V. Barone, B. Mennucci, G. A. Petersson, H. Nakatsuji, M. Caricato, X. Li, H. P. Hratchian, A. F. Izmaylov, J. Bloino, G. Zheng, J. L. Sonnenberg, M. Hada, M. Ehara, K. Toyota, R. Fukuda, J. Hasegawa, M. Ishida, T. Nakajima, Y. Honda, O. Kitao, H. Nakai, T. Vreven, J. A. Montgomery, Jr., J. E. Peralta, F. Ogliaro, M. Bearpark, J. J. Heyd, E. Brothers, K. N. Kudin, V. N. Staroverov, T. Keith, R. Kobayashi, J. Normand, K. Raghavachari, A. Rendell, J. C. Burant, S. S. Iyengar, J. Tomasi, M. Cossi, N. Rega, J. M. Millam, M. Klene, J. E. Knox, J. B. Cross, V. Bakken, C. Adamo, J. Jaramillo, R. Gomperts, R. E. Stratmann, O. Yazyev, A. J. Austin, R. Cammi, C. Pomelli, J. W. Ochterski, R. L. Martin, K. Morokuma, V. G. Zakrzewski, G. A. Voth, P. Salvador, J. J. Dannenberg, S. Dapprich, A. D. Daniels, O. Farkas, J. B. Foresman, J. V. Ortiz, J. Cioslowski and D. J. Fox, Gaussian, Inc., Wallingford CT, 2013, Gaussian 09, Revision E.01.
- [2] (a) C. Lefebvre, G. Rubez, H. Khartabil, J. C. Boisson, J. Contreras-Garcia and E. Henon, *Phys. Chem. Chem. Phys.*, 2017, **19**, 17928-17936; (b) T. Lu and F. Chen, *J. Comput. Chem.*, 2012, **33**, 580-592.
- [3] W. Humphrey, A. Dalke and K. Schulten, *J. Mole. Graph.* 1996, **14**, 33-38.
- [4] X. Gao, S. Bai, D. Fazzi, T. Niehaus, M. Barbatti, W. Thiel, *J. Chem. Theory Comput.*, 2017, **13**, 515-524.
- [5] Z. Mao, Z. Yang, C. Xu, Z. Xie, L. Jiang, F. L. Gu, J. Zhao, Y. Zhang, M. P. Aldred and Z. Chi, *Chem. Sci.*, 2019, **10**, 7352-7357.
- [6] Q. S. Zhang, J. Li, K. Shizu, S. P. Huang, S. Hirata, H. Miyazaki and C. Adachi, *J. Am. Chem. Soc.*, 2012, **134**, 14706-14709.
- [7] M. K. Etherington, F. Franchello, J. Gibson, T. Northey, J. Santos, J. S. Ward, H. F. Higginbotham, P. Data, A. Kurowska and P. L. Dos Santos, *Nat. Commun.*, 2017, **8**, 14987.
- [8] A. Köhler, H. Bässler, *Electronic Processes in Organic Semiconductors, An Introduction*, John Wiley & Sons, 2015.
- [9] B. Valeur, M. N. Berberan-Santos, *Molecular Fluorescence: Principles and Applications*, 2012.
- [10] X. Chen, C. Xu, T. Wang, C. Zhou, J. Du, Z. Wang, H. Xu, T. Xie, G. Bi, J. Jiang, X. Zhang, J. N. Demas, C. O. Trindle, Y. Luo and G. Zhang, *Angew. Chem. Int. Ed.*, 2016, **55**, 9872-9876.

Author Contributions

Zhan Yang, Zhu Mao, Juan Zhao, Yi Zhang, and Zhenguo Chi designed the experiments. Zhan Yang, Zhu Mao, Eethamukkala Ubba, Qiuyi Huang, Wenlang Li and Junru Chen performed the experiments. Zhan Yang and Zhu Mao carried out the theoretical calculations. All the authors were involved in the analysis and interpretation of data. Zhu Mao and Zhan Yang wrote the manuscript with the help of Juan Zhao, Yi Zhang and Zhenguo Chi.